Engineering xxx (xxxx) xxx

Contents lists available at ScienceDirect

Engineering

journal homepage: www.elsevier.com/locate/eng

Research
Medical Engineering—Article

Salmonella-Delivered COBRA-HA1 Antigen Derived from H1N1 Hemagglutinin Sequences Elicits Broad-Spectrum Protection Against Influenza A Subtypes

Ram Prasad Aganja [a], Amal Senevirathne [b], Chandran Sivasankar [a], John Hwa Lee [a,*]

[a] Department of Veterinary Public Health, College of Veterinary Medicine, Jeonbuk National University, Iksan 54596, Republic of Korea
[b] Department of Preventive Medicine, College of Veterinary Medicine, Chungnam National University, Daejeon 34134, Republic of Korea

ARTICLE INFO

Article history:
Received 15 January 2023
Revised 18 June 2023
Accepted 1 August 2023
Available online 15 August 2023

Keywords:
COBRA
Influenza A
Salmonella
Vaccine
Broad spectral protection

ABSTRACT

A universal vaccine is in high demand to address the uncertainties of antigenic drift and the reduced effectiveness of current influenza vaccines. In this study, a strategy called computationally optimized broadly reactive antigen (COBRA) was used to generate a consensus sequence of the hemagglutinin globular head portion (HA1) of influenza virus samples collected from 1918 to 2021 to trace evolutionary changes and incorporate them into the designed constructs. Constructs carrying different HA1 regions were delivered into eukaryotic cells by *Salmonella*-mediated bactofection using a Semliki Forest virus RdRp-dependent eukaryotic expression system, pJHL204. Recombinant protein expression was confirmed by Western blot and immunofluorescence assays. Mice immunized with the designed constructs produced a humoral response, with a significant increase in immunoglobulin G (IgG) levels, and a cell-mediated immune response, including a 1.5-fold increase in $CD4^+$ and $CD8^+$ T cells. Specifically, constructs #1 and #5 increased the production of interferon-γ (IFN-γ) producing $CD4^+$ and $CD8^+$ T cells, skewing the response toward the T helper type 1 cell (Th1) pathway. Additionally, interleukin-4 (IL-4)-producing T cells were upregulated 4-fold. Protective efficacy was demonstrated, with up to 4-fold higher production of neutralizing antibodies and a hemagglutination inhibition titer > 40 against the selected viral strains. The designed constructs conferred a broadly protective immune response, resulting in a notable reduction in viral titer and minimal inflammation in the lungs of mice challenged with the influenza A/PR8/34, A/Brisbane/59/2007, A/California/07/2009, KBPV VR-92, and NCCP 43021 strains. This discovery revolutionizes influenza vaccine design and delivery; *Salmonella*-mediated COBRA-HA1 is a highly effective in vivo antigen presentation strategy. This approach can effectively combat seasonal H1N1 influenza strains and potential pandemic outbreaks.

1. Introduction

Influenza viruses circulate worldwide, causing infections that range from seasonal flu to pandemics with high socioeconomic and medical burdens [1,2]. Protection against influenza is primarily mediated by neutralizing antibodies (Nabs); however, viruses are in constant evolution, frequently altering their antigenic epitopes through antigenic drift to evade the Nabs present in their hosts, creating a great challenge for efficacious vaccine development [3]. The current vaccination strategy is based on seasonal variations in the hemagglutinin (HA) and neuraminidase (NA) sequences of field-isolated strains, but its efficacy is constantly undermined by enormous antigenic variations in the circulating viral strains [4]. Thus, new approaches are required to provide broad protection and long-lasting immunity. Several groups of researchers have focused on developing a vaccine construct using more conserved antigens, such as matrix proteins and nuclear proteins, but the immune responses generated by those antigens were insufficient to protect against influenza infection or prevent morbidity and mortality upon high levels of influenza challenge [5,6]. Therefore, the benchmark for protective immune responses against influenza is still set by HA-specific antibody responses [7].

* Corresponding author.
E-mail address: johnhlee@jbnu.ac.kr (J.H. Lee).

https://doi.org/10.1016/j.eng.2023.08.001

Please cite this article as: R.P. Aganja, A. Senevirathne, C. Sivasankar et al., *Salmonella*-Delivered COBRA-HA1 Antigen Derived from H1N1 Hemagglutinin Sequences Elicits Broad-Spectrum Protection Against Influenza A Subtypes, Engineering, https://doi.org/10.1016/j.eng.2023.08.001

HA is an integral membrane glycoprotein formed when cellular proteases cleave the non-covalent homo-trimer protein HA0 [8]. HA comprises the HA1 and HA2 subunits. The immunodominant but highly variable globular head region is formed by the HA1 subunit, and both subunits contain a relatively conserved stem region. The globular domain is primarily constituted by a membrane-distal receptor binding site (RBS) that attaches to a sialic acid receptor of the host [9,10]. Although the glycosylation patterns and surface properties of the influenza subtypes vary extensively, the highly conserved structural integrity of HA ensures that exposure to the HA head domain will elicit a broad-spectrum immune response [11]. One reasonable strategy to overcome the antigenic drift and mismatch that afflict current influenza vaccines for pandemic and seasonal viral strains could be using multiple rounds of consensus building to generate a candidate that reflects traces of evolution over a long period, a method known as computationally optimized broadly reactive antigen (COBRA) [12–14]. With that method, we used H1N1 sequences derived from humans, birds, and swine between 1918 and 2021 and developed a consensus HA sequence that incorporated diversified epitopes to eliminate the potential biases of a sequence selected from a single outbreak, source of collection, or time frame.

Conventional influenza vaccine production is based on culturing the virus in an embryonated egg and subsequently inactivating it [15], which is a lengthy, time-consuming process. Furthermore, evidence indicates that viral mutation can occur during egg-based virus production, reducing the effectiveness of the resulting vaccine, which demands consistency in antigen production [16]. On the other hand, cell culture-based vaccine production, which is currently popular, requires a sophisticated lab and has high costs while yielding low quantities of vaccine. To resolve those issues, *Salmonella* can be used as an influenza vaccine delivery system because it is economically compatible with industrial-scale production, free from classical egg-based methods, and free from the need for sophisticated viral propagation techniques, making it a suitable choice for future mass production. *Salmonella* with a hyper-invasive and hyper-immunogenic phenotype was developed for plasmid delivery by deleting the *lon* and *cpxR* genes from *Salmonella* pathogenicity island I (SPI1) and the *sifA* gene from SPI2 [17–19]. To ensure safety, aspartate semialdehyde dehydrogenase (*asd*)gene auxotrophic deletion was used instead of antibiotic selection markers, forming *Salmonella* JOL2500. To arrive at seamless antigenic expression, we used a viral RNA-dependent RNA polymerase-based eukaryotic expression plasmid (RdRp-eep) vector, pJHL204 vector, that delivers and enhances gene expression of the desired antigen in the cytoplasm [20,21]. Because *Salmonella* can survive intracellularly, it can release its plasmids into cells. The design of the pJHL204 vector leverages the Semliki Forest virus (SFV) replicon for antigen expression. This vector is composed of genes encoding SFV non-structural proteins (nsp 1–4) that generate a replicase complex responsible for multiplying antigen-coding messenger RNA (mRNA), enabling efficient expression through RNA self-replication [22]. This system is created by using the cytomegalovirus (CMV) promoter to initiate transgene expression. Thus, attenuated *Salmonella* JOL2500 carrying the constructed sequence coding HA1 in an RdRp-eep vector was designed as a vaccine candidate to replace the seasonal reformulation of the influenza vaccine.

Our goal in this study was to develop vaccine candidates using an appropriate consensus sequence designed based on COBRA to induce a broad-spectrum immune response. Therefore, we created antigen constructs from different regions of the HA1 consensus sequence using the COBRA method, and we used an RdRp-eep vector and attenuated *Salmonella* JOL2500 to efficiently express and deliver the antigen, respectively. We found that the COBRA-HA1 delivered by *Salmonella* elicited an immune response against influenza infection in a mouse model. Thus, we have demonstrated that the functional expression of COBRA-HA1 protects mice from infection by heterologous, highly pathogenic influenza variants: A/PR8/34, A/Brisbane/59/2007, A/California/07/2009, KBPV VR-92, and NCCP 43021.

2. Materials and methods

2.1. Design and selection of vaccine construct

More than 4800 HA1 sequences from H1N1 influenza virus isolated from humans, birds, and swine between 1918 and 2021 were retrieved from the National Center for Biotechnology Information (NCBI) Influenza Virus Resource Database [23]. All the sequences were gradually compiled through three layers of consensus to construct the final sequence (Fig. 1(a)). The sequences were grouped by year intervals using BioEdit to generate the first layer of the consensus sequence for human, avian, and swine viruses. The alignments were further consolidated by choosing the most common amino acids (AAs) to develop the second- and third-layer consensus sequences with the maximum likelihood method. The final consensus sequence was derived from all three origins. From the final sequence, regions covering 90–240, 1–240, 100–240, 100–300, and 1–300 AA were selected for further analysis and named constructs #1 to #5, respectively (Fig. 1(b)). The corresponding molecular structure for the final sequence was analyzed using protein structure homology modeling[†]. The accuracy of the model was evaluated by deriving Ramachandran plots for the AAs with a PROCHECK at University of California, Los Angeles[‡] [24]. The linear B cell epitopes of the consensus sequence were predicted by the BepiPred Linear Epitope Prediction tool in the Immune Epitope Database (IEDB) resource [25]. Protein structure validation was conducted on the ProSA-web server[††] by determining the overall quality score of the predicted protein structure. The antigenicity of the designated construct was confirmed by the ANTIGENpro[‡‡] database. The structural integrity of the predicted protein structure for the complete length of the deduced consensus sequence, designated as construct #5, was assessed using the ClusPro 2.0 protein: protein docking method with recognized Nabs with known structures [26]. For that process, we used the CH65 fragment of antigen binding (Fab) (protein databank ID: 4WUK) head-neutralizing monoclonal antibody (MAb), which specifically interacts with the receptor-binding domain. Then, the binding score was estimated using Frodock software [27]. For comparison, a globular head from the 2009 pandemic H1N1 HA (rcsb_pdb_3UYX) was used as a reference structure.

2.2. Bacterial strains, plasmids, and primers

The bacterial strains and plasmids used in this study are listed in Table S1 in Appendix A. All bacterial strains were routinely grown in Luria Bertani (BD; Sparks, USA) medium at 37 °C. The attenuated *Salmonella typhimurium* (ST) strain JOL2500, with the deletion of the *lon*, *cpxR*, *sifA*, and *asd* genes, was used as the vaccine delivery system.

2.3. Preparation of the vaccine construct

The consensus sequence of the HA1 gene designed using the COBRA method was chemically synthesized (Bioneer, Republic of

[†] https://swissmodel.expasy.org.
[‡] https://saves.mbi.ucla.edu/.
[††] https://prosa.services.came.sbg.ac.at/prosa.php.
[‡‡] http://scratch.proteomics.ics.uci.edu.

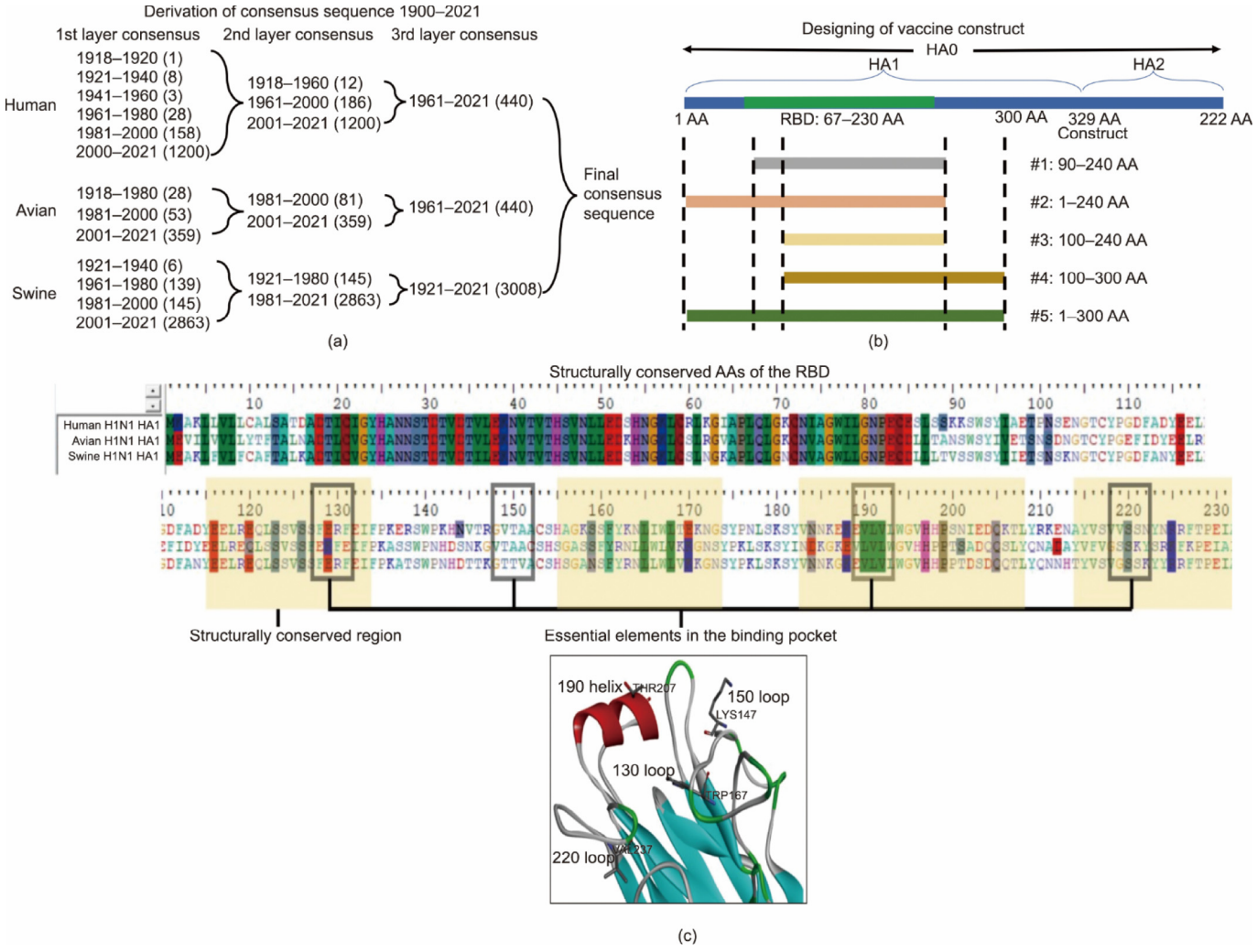

Fig. 1. Design and selection of influenza A hemagglutinin globular head (HA1) region. (a) A schematic representation of consensus sequence derivation by forming layers using COBRA. From thousands of sequences, three layers of consensus were built in BioEdit and used to construct the final consensus sequence of the HA1 of influenza A. (b) Selection of different sections of the globular head region of the H1N1 HA sequence. Construct #5 encompasses a complete length of the consensus sequence, including the N-terminus signal sequence, C-terminus stalk portion, and the globular head region. Construct #1 covers the RBS and globular head region, with an exemption of glycosylation sites except at 95. Construct #2 incorporates proximal antigenic receptor sites and the RBS. Construct #3 covers only the core interaction part of the HA molecule (RBS of the globular head region). Likewise, construct #4 was built with the relatively conserved stalk portion of the HA molecule and the RBS. (c) A schematic representation of AAs of the receptor binding domain (RBD) structurally conserved from human, avian, and swine origin. The yellow highlighted regions are structurally conserved regions, and AAs inside the box represent the essential elements in the binding pockets. THR: threonine; TRP: tryptophan; LYS: lysine; VAL: valine.

Korea) to obtain constructs #1 and #5. The designed gene fragments were cloned into pJHL204 using the AscI and PacI restriction sites and transformed into *Salmonella* JOL2500 by electroporation. Vaccine candidates carrying constructs #1 and #5 were labeled *Salmonella* JOL2781 and JOL2786, respectively. Constructs #2 to #4 were synthesized from construct #5 by polymerase chain reaction (PCR) amplification and prepared as vaccine candidates JOL2783, JOL2784, and JOL2785, respectively. Vaccine candidates are represented using their respective construct numbers for convenience. JOL2500 containing only pJHL204 served as the vector control (VC), JOL2865.

2.4. Animals and ethics statement

All experiments using mice were approved by the Jeonbuk National University Animal Ethics Committee (JBNU-2021–027) following guidelines of the Korean Council on Animal Care and the Korean Animal Protection Law, 2007: Article 13. Six-week-old, specific pathogen-free female BALB/c mice procured from Samtako, Republic of Korea, were maintained on a standard feeding regimen of antibiotic-free food and water ad libitum at the Animal Housing Facility of the College of Veterinary Medicine, Jeonbuk National University.

2.5. Cell lines and viruses

RAW 264.7, HEK293T, and MDCK cell lines were procured from American Type Culture Collection and maintained in Dulbecco's modified Eagle's medium (DMEM; Lonza, Switzerland) supplemented with 10% fetal bovine serum (FBS; Gibco, USA), 100 units·mL^{-1} penicillin, and 100 μg·mL^{-1} streptomycin at 37 °C in 5% CO_2. The RAW 264.7 and HEK293T cells were used for the protein expression study. The MDCK cells were used to propagate the influenza A/PR8/34, A/Brisbane/59/2007, A/California/07/2009, KBPV VR-92, and NCCP 43021 virus strains and to estimate the viral titer as 50% tissue culture-infectious dose ($TCID_{50}$). Viruses were stored at −80 °C until use.

2.6. Expression and purification of recombinant protein and preparation of antibodies

The target antigenic recombinant proteins were expressed in an *Escherichia coli* (*E. coli*) DE3 host following the standard cloning procedure. Briefly, the target genes were cloned into pET28a(+), and the *E. coli* DH5-α strain was transformed with the cloned plasmid. Then, the plasmid with the desired genes was extracted, PCR-confirmed, and used to transform *E. coli* BL21 (DE3). Bacterial cultures were induced to express recombinant proteins with 1 mmol·L^{-1} isopropyl-β-*D*-thiogalactopyranoside (IPTG) for 4 h at 37 °C, and that expression was confirmed by sodium dodecyl sulfate polyacrylamide gel electrophoresis (SDS-PAGE). The recombinant proteins were purified using nickel-nitrilotriacetic acid column chromatography (Takara, Japan) with the urea lysis method. The purified recombinant proteins for constructs #1 and #5 were inoculated into rabbits to raise polyclonal antibodies against the proteins, as described elsewhere [28].

2.7. Expression of vaccine constructs

In vivo expression of the antigens was studied in RAW 264.7 and HEK293T cells cultured in six-well plates. Monolayer cells were transfected with *Salmonella* carrying constructs #1 to #5 at 40 multiplicity of infection for 2 h, and non-invading extracellular *Salmonella* was eliminated by gentamycin (100 μg·mL^{-1}) treatment for 2.5 h [21]. Cells were replenished with 2% FBS-enriched DMEM and incubated for 48 h. Then, the cells were harvested and analyzed for expression by reverse transcription PCR (RT-PCR), Western blotting, and an immunofluorescence assay (IFA). Total RNA was extracted using the Trizol method (GeneAll, Republic of Korea) and converted into complementary DNA (cDNA) by RT-PCR. Then, PCR amplification was done to confirm the full-length expression of all constructs. For western blotting, RAW 264.7 cells were harvested in radio immunoprecipitation assay (RIPA) lysis buffer and subjected to sonication for 5 s at 50% amplitude for 2–4 cycles, with a 60 s gap between cycles. The supernatants were collected, subjected to SDS-PAGE (12%), and transferred to a polyvinylidene fluoride (PVDF) membrane (ImmobilonR-P; Millipore, Ireland). The membrane was treated with primary antibody from rabbits (1:500 dilution) and incubated with horseradish peroxidase (HRP)-conjugated anti-rabbit immunoglobulin G (IgG) secondary antibody (1:6000; SouthernBiotech, USA), and then the images were developed by adding a chemiluminescent substrate. The developed images were documented for further analysis (Cytiva, USA).

In addition, protein expression in RAW 264.7 cells was validated by IFA. After 48 h of incubation, the bactofected cells were fixed with chilled acetone (80%) at −20 °C for 10 min. The fixed cells were permeabilized with 0.1% Triton X-100 and then blocked with 3% bovine serum albumin. Cells were treated with primary antibodies from rabbits (1:200 dilution) at 4 °C overnight, and then they were washed and stained with Alexa Fluor 488-conjugated donkey anti-rabbit IgG (Invitrogen, USA) at 1:5000 dilution. Next, the cells were stained with 4′,6-diamidino-2-phenylindole (DAPI) for nuclear spotting (Sigma-Aldrich, Germany) and observed for bright, green fluorescence and blue staining under a Leica fluorescence microscope (Leica Biosystems, Germany) the images were documented.

2.8. Localization of ST and safety assessment of vaccine constructs

Six-week-old female mice (N = 9) were each treated intramuscularly with 1×10^7 *Salmonella* carrying construct #5 prepared in 100 μL of phosphate-buffered saline (PBS) or with PBS only (control group) and monitored until the end of the experiment for adverse effects such as weight loss, diarrhea, irritability, ruffled fur, deterioration in health, and reduction of food intake. Spleen and liver samples were collected from three mice per group that were sacrificed at 3, 7, and 14 days post-inoculation (dpi) and subjected to bacterial quantification by plating on brilliant green agar. Equal amounts of tissue samples were homogenized separately in PBS using a mechanical homogenizer (IKA ULTRA-TURRAX; Merck, Germany) and plated at 10-fold serial dilutions. Colonies were enumerated, and representative colonies were confirmed to be *Salmonella* carrying construct #5 by PCR with specific primers.

The remaining tissue samples from each animal were examined using histopathological and immunohistochemical analyses to determine tissue deterioration and ST localization. For these experiments, organs were first harvested and preserved in a formaldehyde solution (10%). The samples were embedded in paraffin and sectioned (2 μm). Tissue sections were stained with hematoxylin and eosin (H&E) to examine the histopathology and extent of damage to the spleen and liver. ST localization was detected by immunohistochemical staining with anti-*Salmonella* rabbit antibodies following the standard protocol. Briefly, specimens were deparaffinized with xylene and subsequently hydrated with an ethanol gradient and distilled water. Then, the specimens were heated in citrate buffer (pH 6) at 100 °C for 30 min to retrieve the antigens, which was followed by the addition of 0.3% methanolic H_2O_2 to inhibit peroxidase activity. The samples were consecutively labeled with primary antibodies raised in a rabbit (1:200 dilution) and treated with HRP-conjugated goat anti-rabbit antibody (1:3000 dilution). Finally, 3,3′-diaminobenzidine (DAB; Sigma-Aldrich) was added to develop color, and the images were documented.

2.9. Immunization

Eight mice per group were immunized with the vaccine candidates (*Salmonella*-carrying constructs) by the intramuscular route at a dose of 1×10^7 colony forming units (CFU) per mouse. Similarly, ST carrying the empty vector (JOL2865) was administered in the VC group, and the healthy control group received PBS treatment. At 21 dpi, five mice from each group were sacrificed, and splenocytes were collected, as described elsewhere [29]. Changes in body weight were monitored in the remaining mice until 28 dpi to assess the effects of inoculation.

2.10. Enzyme-linked immunosorbent assay (ELISA)

Sera were collected from immunized mice (five mice per group) at 21 dpi, and total IgG, IgG1, and IgG2a were measured by ELISA. Briefly, 96-well ELISA plates (Greiner Bio-One, Austria) were coated with recombinant proteins (5 μg·mL^{-1} in carbonate-bicarbonate buffer, pH 9.6) and incubated at 4 °C overnight. The wells were blocked with 5% skim milk, washed with PBS containing 0.1% Tween 20, and incubated with serum samples for 1 h at 37 °C. The samples were washed and incubated at 37 °C for 1 h with HRP-conjugated goat anti-mouse IgG, IgG1, and IgG2a antibodies at 1:5000 dilution to determine the concentrations of the respective antibodies. Finally, color was developed with freshly prepared o-phenylenediamine dihydrochloride substrate. The reaction was stopped by adding 3 mol·L^{-1} H_2SO_4, and optical density (OD) was measured at 492 nm using a microplate reader (Tecan, Switzerland). All experiments were conducted in triplicate.

2.11. Fluorescent-assisted cell sorting (FACS) and splenocyte proliferation assay

Splenocytes were aseptically harvested from mice (five mice per group) and cultured in Roswell Park Memorial Institute (RPMI)

medium supplemented with 10% FBS for the FACS analysis, splenocyte proliferation assays, and cytokine measurement. Cells were cultured in a 96-well plate for the FACS and splenocyte proliferation assays and in a 12-well plate for cytokine measurement. The cells were stimulated with recombinant proteins (400 ng·well^{-1}) for 72 h at 37 °C in a 5% CO_2 incubator. The change in T lymphocyte subsets following immunization was ascertained with flow cytometry by staining splenocytes with phycoerythrin (PE)-labeled anti-CD3e, PerCPVio700-labeled anti-CD4, and fluorescein isothiocyanate (FITC)-labeled anti-CD8a anti-mouse antibodies (Miltenyi Biotec, Germany). In addition, to evaluate the expression of intracellular cytokines (interferon-γ (IFN-γ) and interleukin-4 (IL-4)), splenocytes from mice treated with constructs #1 and #5 were stimulated with recombinant proteins. The intracellular cytokines were retained by brefeldin A treatment for 4 h. T lymphocytes were initially labeled with CD4 and CD8 and then separately treated with PE-labeled anti-IFN-γ (Miltenyi Biotec) and PE-labeled IL-4 (BioLegend, USA) anti-mouse antibodies, following the manufacturers' instructions. The $CD3^+CD4^+$ and $CD3^+CD8^+$ T cell subpopulations were gated from $CD3^+$ cells (Fig. S1 in Appendix A), and the IFN-γ- and IL-4-producing cells within the T lymphocyte population were quantified using a MACS Quant analysis system (Miltenyi Biotec).

3-(4,5-dimethylthiazol-2-yl)-2,5-diphenyltetrazolium bromide (MTT) chromophore solution was added to splenocytes to determine the proliferation induced by the recombinant protein. The proliferation index was calculated by dividing the absorbance at 570 nm (A570) values from immunized mice by those from control mice [30]. This experiment was conducted in triplicate.

2.12. Cytokine responses

Splenocytes stimulated with recombinant proteins were harvested to extract total RNA using a RNeasy mini kit (Qiagen, Germany) according to the manufacturer's instructions. Then, cDNA was synthesized from 1 μg of purified RNA (Elpis Biotech, Republic of Korea). The expression of cytokines (IFN-γ, tumor necrosis factor-α (TNF-α), IL-10, IL-4, and IL-17) was measured at the mRNA level with Applied Biosystems (#4367659; Applied Biosystems, USA) using SYBR green PCR master mix (Elpis Biotech) as previously described. The primers used for this study are listed in Table S2 in Appendix A [31]. A melting peak analysis was performed to confirm the absence of contamination and the specificity of the PCR amplification. The $2^{-\Delta\Delta CT}$ method was used to determine changes in mRNA levels, with β-actin as the internal control [32].

2.13. Virus neutralization assay

Neutralization of the virus was measured using a microneutralization (MN) assay described elsewhere [33]. Collected sera were heat-inactivated at 56 °C for 30 min, and serial dilution was done with a dilution factor of 2. The diluted serum samples were incubated with 200 $TCID_{50}$ of H1N1 PR8/34 for 1 h at 37 °C. The mixtures were allowed to form antibody virus complexes and added to MDCK cell monolayers in 96-well plates. The cells were incubated in a humidified CO_2 incubator at 37 °C for 72 h and monitored daily for 3 days using a microscope to determine the cytopathic effects (CPEs). The neutralizing antibody titer was recorded as the highest serum dilution that resulted in complete CPE inhibition in two out of three wells. Similarly, the virus neutralization titer was estimated for the H1N1 A/Brisbane/59/2007, A/California/07/2009, KBPV VR-92, and NCCP 43021 strains.

2.14. Hemagglutination inhibition (HI) assay

A HI assay was performed to quantify the ability of each serum to agglutinate erythrocytes. The HI test was conducted with 0.75% chicken erythrocytes. A serial twofold dilution of heat-inactivated serum (inactivation at 56 °C for 30 min) was treated with four hemagglutination units, equivalent to a virus described in the World Health Organization (WHO) manual for laboratory influenza surveillance [34]. The HI titer was determined as the reciprocal of the last well without agglutination. These assays were conducted in duplicate.

2.15. Challenge of immunized mice

To test the protective efficacy of our system, immunized mice (eight mice per group) from all groups and controls were challenged intranasally with the influenza A virus. For this study, mice were challenged with a lethal dose (1×10^6 mean embryo infective dose (EID_{50})) of H1N1 influenza A/PR/8/34 virus two weeks after their booster immunization. For the broad spectral protection study, mice immunized with vaccine constructs #1 and #5 were challenged with the influenza A/Brisbane/59/2007, A/California/07/2009, KBPV VR-92, and NCCP 43021 strains 28 days after their initial immunization. The challenged mice were handled following standard guidelines and monitored daily for signs of systemic infection, changes in body weight, and mortality. Mice (five mice per group) were sacrificed on day 3 after virus inoculation, and their lungs were collected to determine morphological deterioration and viral titers. The gross analysis of the harvested lungs was rated for disease severity based on the lungs of naïve mice as the control and scored as 0 for no change and 1 to 3 for mild, moderate, and severe complications, respectively.

Lung tissue was collected in RiboEx for viral RNA isolation using the Trizol method. The viral RNA copy number was determined by extracting RNA, converting it into cDNA, and performing quantitative RT-PCR (qRT-PCR) with the viral RNA as a standard for comparison, as previously described [35]. Histopathological changes in the lungs were determined by H&E staining following the procedure described above. The location of the viral particles was determined using the immunohistochemistry (IHC) method described earlier with rabbit polyclonal antibodies.

2.16. Statistical analysis

All data were analyzed using GraphPad Prism 9.0 software (GraphPad, USA). One-way analysis of variance (ANOVA) with Dunnett's multiple comparisons test was conducted to determine statistical differences among the vaccinated and control groups. *P* values < 0.05 were considered statistically significant.

3. Results

3.1. Construct design and in silico analysis

More than 4800 HA sequences from influenza virus genomes were retrieved from the NCBI influenza database, which spans from 1918 to 2021 and covers H1N1 isolates of human, avian, and swine origin. All sequences were gradually compiled to derive sequential consensus sequences that we eventually condensed into a single sequence (Fig. 1). The structural integrity of the protein for the final consensus sequence was analyzed using bioinformatics tools. When we assessed the accuracy of the model by deriving a Ramachandran plot of the protein, we found a complete absence of outlier AAs in disallowed regions. In addition, the modeled structure showed nearly 99% of AA residues in favored and

additionally allowed regions (Fig. 2(a)) [36]. The major portion, represented as yellow highlighted areas in the predicted B cell epitopes, signifies the sequence's potential to elicit a humoral response with the designed protein (Fig. 2(b)). The local structural quality of the predicated structure was analyzed using ProSA-web, which projected an overall quality *Z*-score of −7.04 (Fig. 2(c)). The antigenicity predicted by ANTIGENpro was 0.916077 for the final consensus sequence. An in silico analysis using the Phyre-2 server demonstrated three-dimensional structural similarities with the natural structure of the head globular region of the RBS in the H1N1 influenza A/PR8/34 virus (Fig. 2(d)). Once we had the final consensus sequence analysis, we designed different vaccine constructs that all retained the receptor binding domain (RBD) regions (130 loop, 150 loop, 190 helix, and 220 loop structure). The constructs were designed to encompass different regions of HA1. Construct #5 encompasses a complete length of the consensus sequence from the N-terminus signal sequence to the C-terminus stalk portion, including the globular head region. Construct #1 covers the RBS and the globular head region, with an exemption of glycosylation sites except at 95, which is found in almost all H1 viruses. Construct #2 was selected to incorporate proximal antigenic receptor sites and the RBS by terminating the C-terminal region of the stalk from construct #5. This region is highly conserved and plays a role in membrane fusion. Likewise, construct #3 covers the RBS of the globular head region as the core interaction part of the HA molecule and was designed to exclude all accessory regions. Construct #4 was built with the relatively conserved stalk portion of HA, along with the RBS, to confer the benefit of broad-spectrum coverage through relatively conserved HA regions. The binding energy between each construct and a well-known recombinant human anti-H1N1 HA antibody, the CH65 Fab that interacts with the RBD, was predicted with the docking method using Frodock software (Figs. 2(e) and (f)) [27]. The binding score of a reference, a globular HA head from the 2009 pandemic influenza A/California/04/2009 (H1N1) strain, was comparable to the score for the designed constructs, which ranged from 2430 to 2900. Thus, the analysis projected reasonable affinity, highest for construct #5, for the CH65 MAb structure (Fig. 2(f)).

3.2. Protein expression

The protein expression of the vaccine constructs in RAW 264.7 and HEK293T cells was evaluated at the mRNA level post-

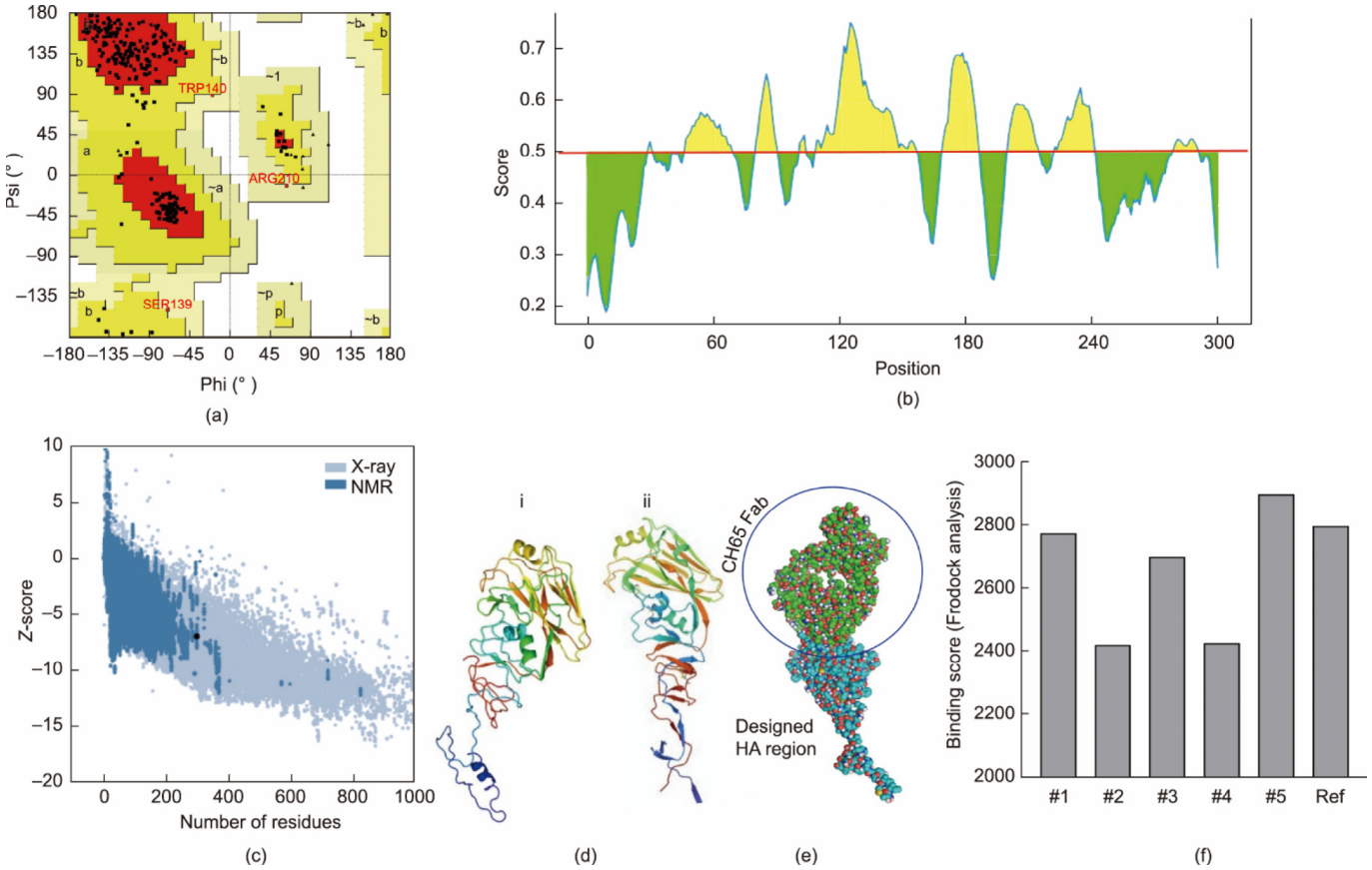

Fig. 2. Structural validation of the predicted protein for the consensus sequence. (a) A Ramachandran plot analysis was performed for the COBRA-derived consensus sequence of 1–300 AA. Black dots represent angles for each residue. The complete absence of outlier AAs confirms that the structures are reasonably stable and suitable for further analysis. Phi represents the C–N bond rotation angle on the left side of the α carbon, while psi represents the C–C bond rotation angle of the α carbon in one peptide unit. A, B, and L represent the region for β sheet, right-handed α-helix, and left-handed α-helix respectively. The red, brown, and yellow regions indicate the most favored (A, B, L), additionally allowed (a, b, l, p), and generously allowed (~a, ~b, ~l, ~p) regions as defined by PROCHECK. (b) The B-cell epitope was predicted using the BepiPred-2.0 epitope predictor. The analysis was conducted in the IEDB repository resource, and the predicted B cell epitopes are represented in yellow above the threshold (red) line. (c) The predicted structure was analyzed by ProSA-web for structural quality and has a Z-score of −7.04, which is in the range of native conformations. (d) Comparison of HA1 structures. The comparative analysis for the (i) predicted model structure of construct #5 from Phyre2 and (ii) HA structure of H1N1 influenza A/PR/8/34 virus (326 AA) showed a similar 3D structure. (e) The binding interaction between the CH65 Fab head-neutralizing monoclonal antibody (MAb) and the receptor-binding domain of sequence #5 derived from COBRA. The specific interaction was illustrated by molecular docking developed from ClusPro 2.0 protein: protein docking [26] and extracted from PyMOL. (f) Graphical illustration of the binding energy predicted by a Frodock analysis between each selected HA globular head region and the CH65 head neutralizing antibody structure. For better comparison, docking scores with the globular head of hemagglutinin from the 2009 pandemic influenza A/California/04/2009 (H1N1) strain were incorporated as a reference (Ref). ARG: arginase; SER: serine; NMR: nuclear magnetic resonance.

bactofection. Cell lysates from cells infected with the vaccine candidates (except for VC JOL2865) exhibited full-length amplification of all the vaccine candidates from the corresponding cDNA, as shown using the RT-PCR method (Figs. 3(a) and (b)). Protein expression was confirmed by western blotting of cell lysates, with protein bands of 17, 26, 16, 22, and 33 kDa corresponding to constructs #1 to #5, respectively (Fig. 3(c)). The bright fluorescence of RAW 264.7 cells infected with the corresponding vaccine strains corroborated protein expression (Fig. 3(d)). Cells infected with the VC showed no green fluorescence.

3.3. Safety assessment and localization of Salmonella

Upon intramuscular administration to mice, the live-attenuated *Salmonella* carrying the vaccine strains caused no untoward symptoms or mortality during the experimental period. There were no local lesions at the site of injection, which ruled out any adverse effects. Changes in the body weights of the immunized mice were monitored, and the differences with the control group were non-significant until the end of the experiment (Fig. 4(a)). The bacterial load in tissue homogenates showed high colonization at 3 and 7 dpi. At 14 dpi, *Salmonella* disappeared from the liver and spleen (Fig. 4(b)), which signifies that the *Salmonella* vaccine strain is relatively safe and precise in its localization of target sites. Minor inflammatory changes and negligible tissue damage were evident in the histopathological analysis of the spleen and liver on day 3 (Fig. 4(c)). The dispersion of red pulp in the spleen noted at 3 dpi was cleared by 14 dpi (data not shown). The localization of *Salmonella* in the spleen and liver was evident through brown spots in the IHC analysis (Fig. 4(d)). *Salmonella* was dispersed in the spleen and concentrated in the liver.

3.4. Humoral immune response

We measured the induction of humoral immune responses at 21 dpi using an indirect ELISA. Mice immunized with the vaccine strains showed increased production of IgG, IgG2a, and IgG1. The increment was particularly prominent in the groups treated with vaccine constructs #1, #2, and #5 (Fig. 5(a)). There was a significant rise in all three measured immunoglobulins for constructs #1 and #5, demonstrating an antigen-specific antibody response. The level of IgG2a was higher than that of IgG1, illustrating a Th1-dominant immune response (Fig. 5(b)). Such an effective stimulation of a humoral response indicates the antigenicity of the expressed consensus sequence.

3.5. Cell-mediated immune response

The cell-mediated immune response was investigated in immunized mice at 21 dpi. Splenocytes re-stimulated with the respective

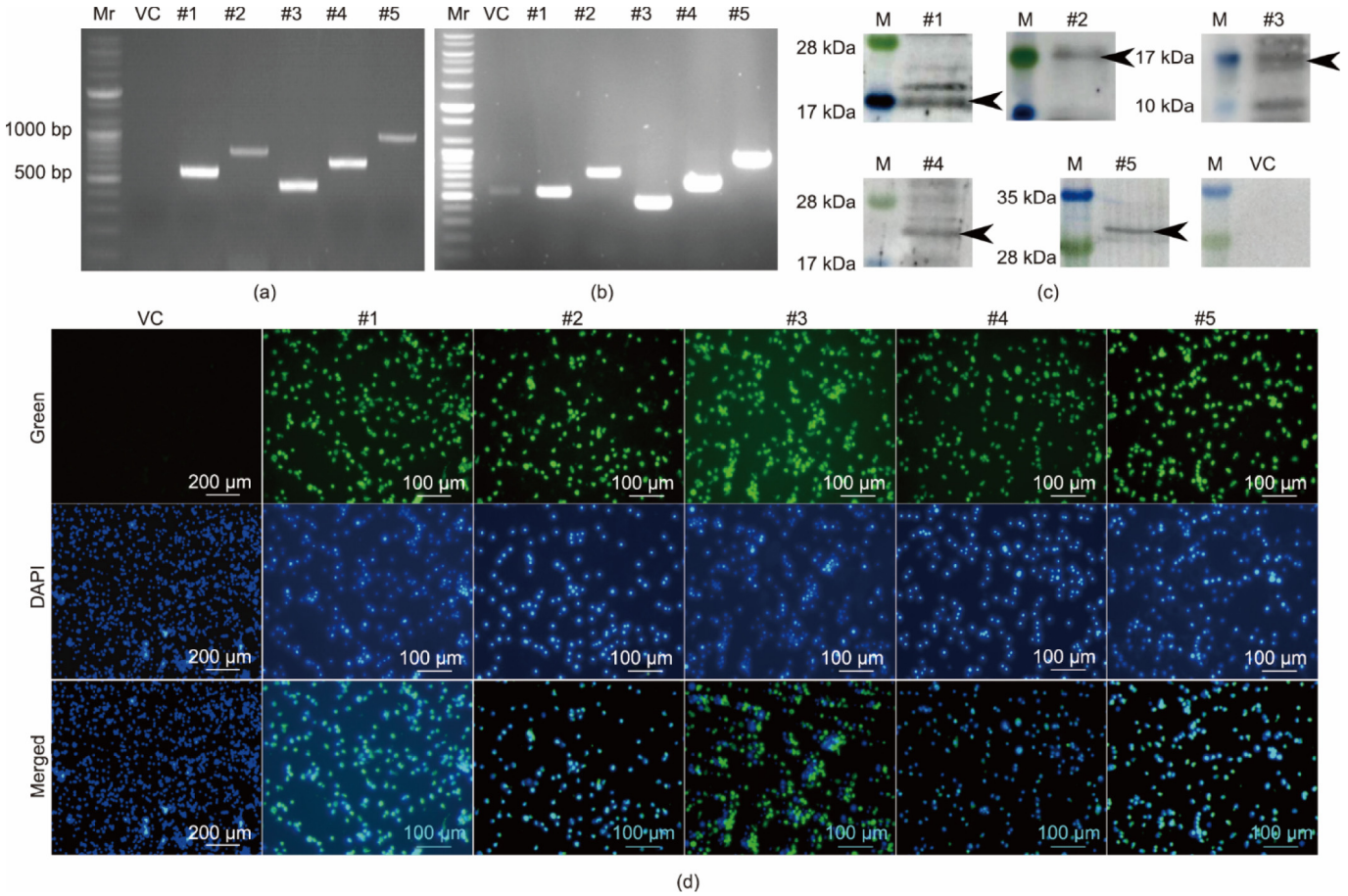

Fig. 3. Expression of proteins. Eukaryotic cell lines were infected with *Salmonella* containing vaccine constructs or the VC. Transcription for recombinant protein expression was evaluated at the RNA level in (a) RAW 264.7 and (b) HEK293T cells. (c) The expression of the recombinant protein in RAW 264.7 cells was detected by western blotting using polyclonal rabbit antisera. Specific immunoreactive bands at 17, 26, 16, 22, and 33 kDa demonstrate expression corresponding to constructs #1 to #5, respectively. No specific band was detected in the VC group. (d) IFA showing the expression of the protein in RAW 264.7 cells. The bright green fluorescence depicted in cells infected with the vaccine constructs confirms the expression of proteins. Such fluorescence was not observed in the VC group. Blue foci indicate nuclei stained with DAPI. Mr: DNA marker; M: protein molecular weight marker.

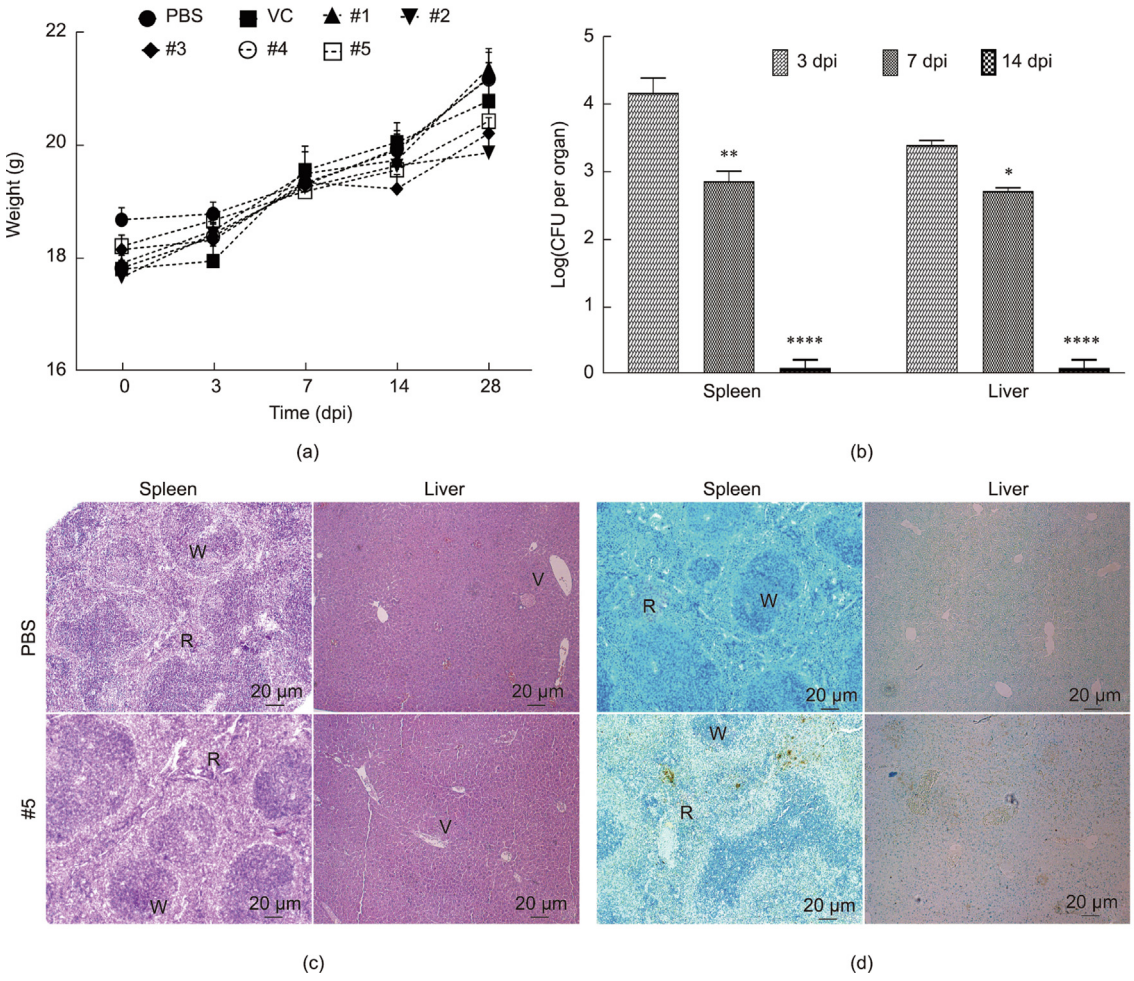

Fig. 4. Safety assessment of the vaccine candidate. Mice were intramuscularly inoculated with ST vaccine constructs at 1×10^7 CFU per mouse. (a) Body weight changes post-immunization. (b) Quantification of bacterial load for construct #5. Bacterial counts dropped significantly by 7 dpi and disappeared by 14 dpi. Data were recovered from three mice per group. (c) Changes in tissue morphology. Histopathological changes in the spleen and liver were examined by H&E staining. Dispersion of red pulp in the spleen and mild to moderate infiltration of inflammatory cells in the liver were noted. (d) Localization of *Salmonella* in tissue. An IHC assay was conducted using an anti-*Salmonella* rabbit polyclonal antibody that captured *Salmonella* localized in the spleen and liver. Brown spots indicate foci of *Salmonella*. R, W, and V denote red pulp, white pulp, and blood vessels, respectively. The data were analyzed using one-way ANOVA with Dunnett's multiple comparisons test. $^*P < 0.05$, $^{**}P < 0.01$, $^{****}P < 0.0001$.

recombinant proteins were examined for changes in the T cell populations, proliferation index, and cytokine profile. The flow cytometric analysis of T cells demonstrated a substantial increase in $CD3^+CD4^+$ and $CD3^+CD8^+$ T cells in mice immunized with vaccine constructs #1, #4, and #5, compared with the PBS group (Fig. 5(c)). The $CD4^+$ T cell population increased by nearly 4% compared with the PBS group in both the construct #1 and construct #5 groups. The immunized groups exhibited a significant increase in splenocyte proliferation, compared with the control group. The proliferative index for all the vaccine strains increased by more than 1.5-fold, and that of construct #4 was the highest (1.66-fold) (Fig. 5(d)). Significant increases in the T cell subpopulations and proliferative index establish a strong T cell-mediated immune recall response.

3.6. Cytokine response

The expression profiles of cytokines was evaluated by qRT-PCR and revealed a significant upregulation of IFN-γ, IL-4, IL-10, and IL-17. The transcripts for IFN-γ expression were highly upregulated, 1.8- to 2.8-fold (Fig. 5(e)). Similarly, the expression of IL-10 was substantially increased, especially with constructs #4 and #5. Except for construct #4, IL-4 expression was prominent for all the vaccine candidates. The upregulation of IL-17 expression was dramatically high, suggesting the activation of Th17 cell populations. To our surprise, the TNF-α level did not increase significantly, which reflects a limited pro-inflammatory response. In general, within the upregulation of Th1 cytokines, IFN-γ expression was higher than that of IL-4, a Th2 cytokine, suggesting a Th1-polarized immune response. Furthermore, the significantly higher $CD4^+IFN\text{-}\gamma^+$ and $CD8^+IFN\text{-}\gamma^+$cell populations driven by constructs #1 and #5 suggest a cell-mediated Th1 response induced by activated T lymphocytes (Fig. 6). The production of $CD4^+IFN\text{-}\gamma^+$ T cells was nearly 2-fold higher for construct #5 (3.25% ± 1.01%) than construct #1 (1.79% ± 0.67%), whereas the $CD8^+IFN\text{-}\gamma^+$ T cell population was slightly higher for construct #5. The expression of the intracellular cytokine IL-4 by T cells from immunized mice was higher than in control mice, demonstrating that the activation of T lymphocytes induces humoral responses through B cell activation as well.

3.7. Serum neutralization and HI

The induction of NAbs against the five selected H1N1 virus strains was evaluated in mouse sera collected at 21 dpi. The sera exhibited CPE inhibition, indicating neutralization of the virus,

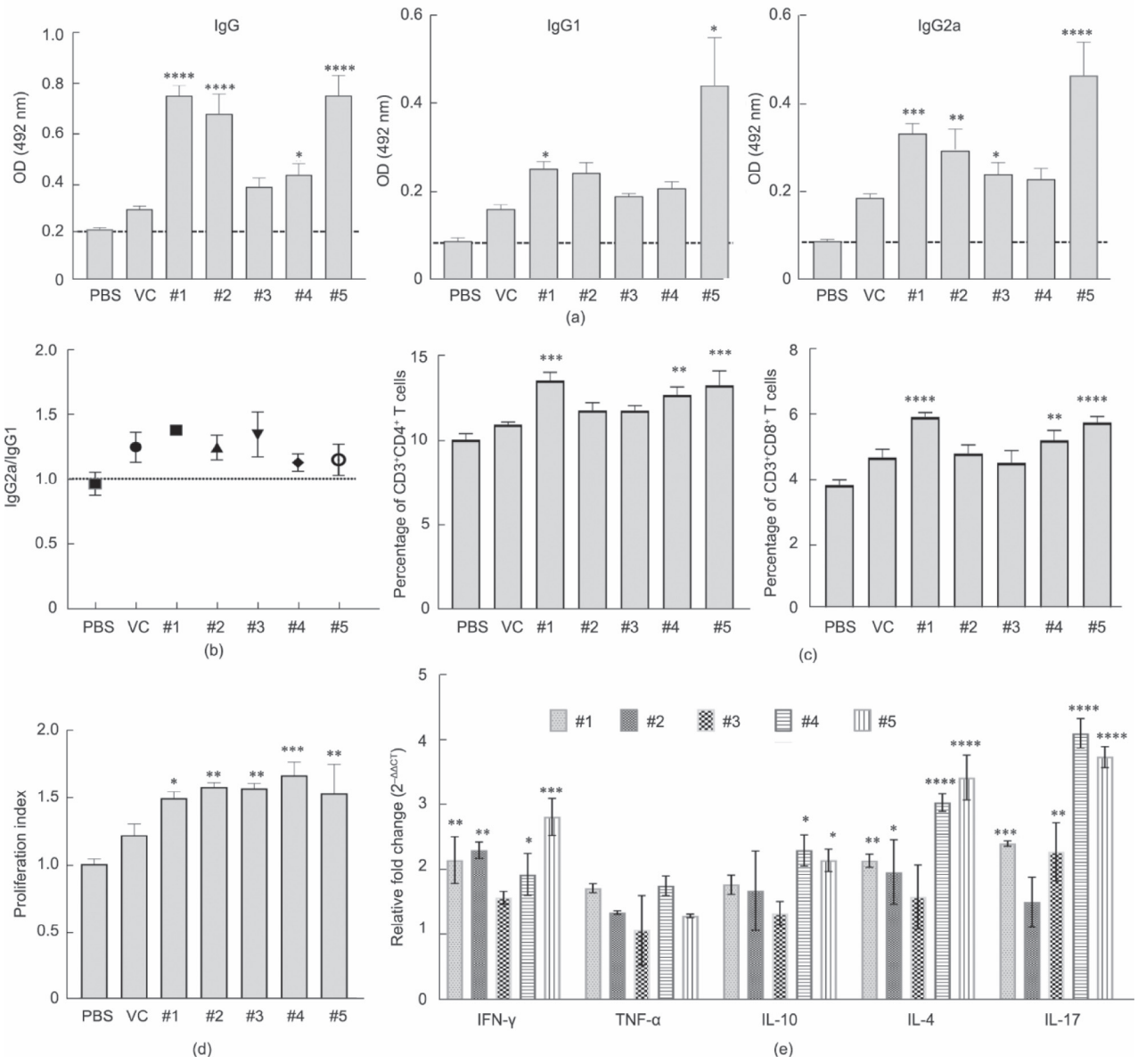

Fig. 5. The immune response elicited in vaccinated mice. (a) Humoral immune response. The sera of mice inoculated with each vaccine construct, PBS, and the VC were collected on day 21 post-immunization and measured for IgG, IgG1, and IgG2a. The antibody titer was measured against purified recombinant proteins. The dotted line indicates the baseline limit of quantification. (b) The ratio of IgG2a and IgG1 is presented to show the Th1-skewed response to immunization. (c) T cell-mediated immune recall response in splenocytes. The data represent changes in the percentage of $CD3^+CD4^+$ and $CD3^+CD8^+$ T cells gated in CD3+ in response to stimulating splenocytes with their respective immunogens. (d) Proliferation index of splenocytes. (e) Cytokine expression levels. Relative fold changes in the expression of cytokines were determined by qRT-PCR 72 h after stimulating splenocytes with recombinant protein. The changes in cytokines were measured at the mRNA transcript level using the $2^{-\Delta\Delta CT}$ method, with β-actin as the internal control. Error bars denote the standard error of mean. Data were analyzed by independent-sample T-testing and ANOVA. $^*P < 0.05$, $^{**}P < 0.01$, $^{***}P < 0.001$, and $^{****}P < 0.0001$.

with an average $\log_2$(titer value) of 6 for constructs #1 and #5. The NAb titer was consistently higher than in the control and VC groups (Fig. 7(a)). To test the strength of antibodies developed post-immunization, HA inhibition at serial dilutions of serum was used to analyze the ability of the virus to agglutinate erythrocytes. The sera collected from immunized mice had a considerably higher HI titer than those from the control mice (Fig. 7(b)). In addition, the presence of CPE in wells treated with sera from the VC immunized group strengthens the finding of NAbs elicited in immunized mice (Fig. 7(c)).

3.8. Challenge and protection

The virus challenge experiment was intended to investigate the protection conferred on the immunized mice against the H1N1 A/PR8/34 virus. The level of protection against the viral challenge was assessed by monitoring the mice for signs of systemic infection in the lungs on the third day after the challenge. A severe drop in body weight was noted post-challenge in the PBS- and VC-immunized mice (Fig. 8(a)). Gross morphological examination of the lungs revealed infection-induced abnormalities, including dark red coloration and pulmonary edema, which was assessed in comparison to the naïve control. There was mild to no inflammation in the lungs of mice immunized with construct #1 or construct #5, with a lung index score of around 1.0 (Fig. 8(b)). The remaining constructs scored higher values, demonstrating minimal protection. A substantial reduction in the viral copy number, compared with the non-immunized and VC groups, was exhibited by mice treated with all the vaccine strains. This implies the potential protective efficacy of the designed vaccine constructs (Fig. 8(c)).

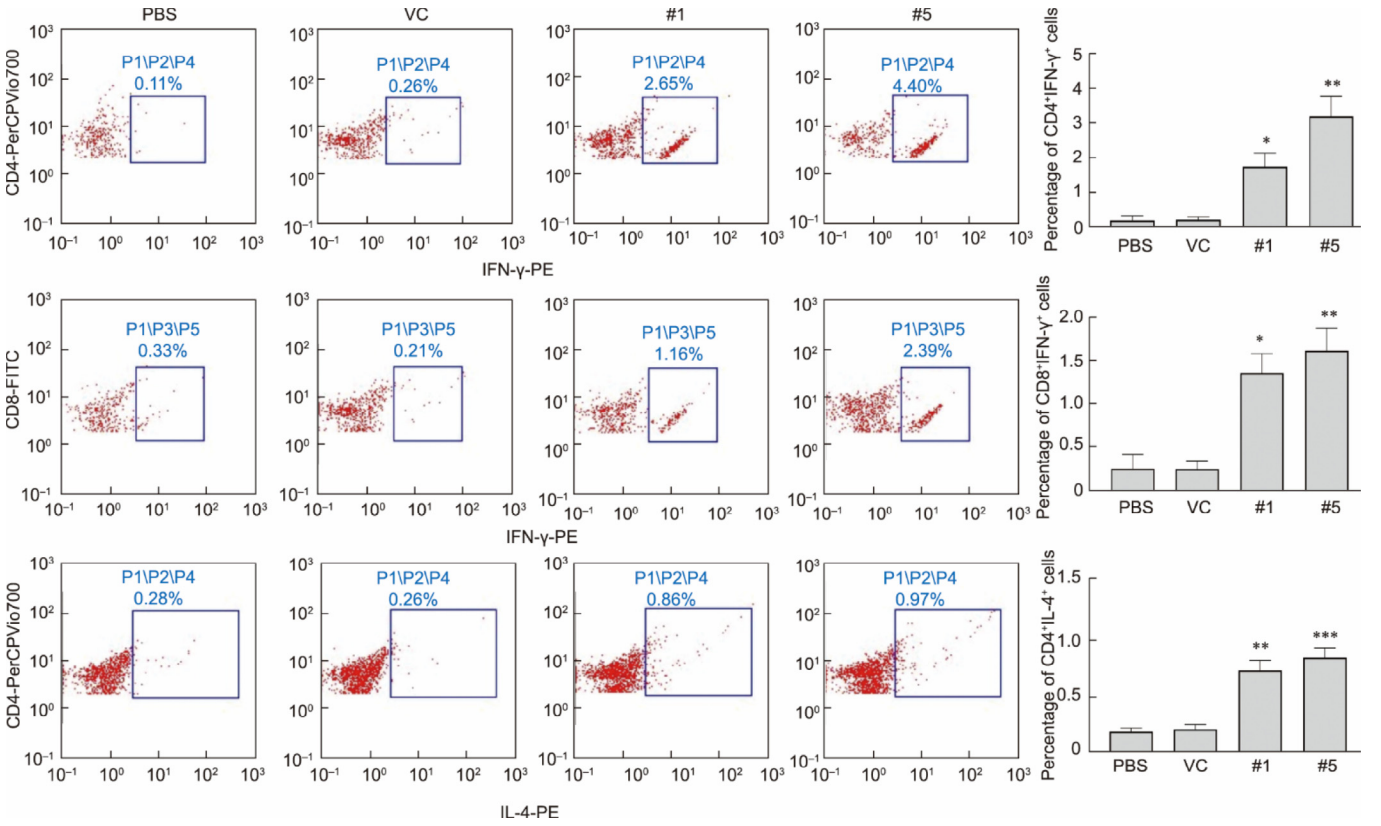

Fig. 6. Expression of intracellular cytokines by T cells after stimulating splenocytes with recombinant protein. $CD4^+$ cells and $CD8^+$ T cells were examined for IFN-γ using a flow cytometer. $CD4^+$ T cells were examined for IL-4 expression. The expression was evaluated for vaccine constructs #1 and #5. Cells were gated under the plots P1 to P5, where P1 to P3 represent lymphocytes, CD4 cells, and CD8 cells respectively. P4 and P5 indicate corresponding positive cells. Data were analyzed by independent-sample T-testing and ANOVA. $^*P < 0.05$, $^{**}P < 0.01$, and $^{***}P < 0.001$.

Consistent morphological observations were recorded from the harvested lungs. We found minimal changes in the lungs of immunized mice, whereas dark lesions were noted in the PBS and VC groups (Fig. 8(d)).

The ability of the designed constructs to provide broad protection was evaluated by challenging immunized mice with different strains of H1N1 virus, namely A/Brisbane/59/2007, A/California/07/2009, KBPV VR-92, and NCCP 43021. The challenged mice exhibited similar outcomes in terms of body weight (Fig. 9(a)). Moreover, immunization resulted in reduced lung damage, as evidenced by a minimum lung score, indicating a protective immune response (Fig. 9(b)). The viral copy number declined significantly, reaching a lower detection level by day 7 post-challenge for influenza A/Brisbane/59/2007, A/California/07/2009, KBPV VR-92, and NCCP 43021 (Fig. 9(c)).

Histopathological analyses of lungs from mice challenged with the viruses revealed dramatic tissue damage in the non-immunized and VC groups. Such tissue distortion was minimal in the lungs of the immunized mice (Fig. 10). The protective efficacy was further confirmed by the IHC analysis of the virus in lung samples. Higher concentrations of virus, shown as brown foci, appeared in the non-immunized and VC groups than in the immunized mice, indicating that immunization reduced the viral load in the lung sections (Fig. 11).

4. Discussion

Continuous antigenic variation caused by evolutionary antigenic drift in circulating viral strains undermines the efficacy of influenza vaccines developed based on seasonal variations in the HA and NA sequences of field-isolated strains. To address the issue of viral escape due to antigenic epitope variation and prevent yearly vaccine reformulation, a broad protective and long-lasting vaccine candidate is required. Therefore, we have proposed a strategic approach called COBRA and targeted the highly variable globular head region, HA1, to find traces of evolution from 1918 to 2021 in strains of human, avian, and swine origin [12–14]. Using this method, we developed a novel vaccine platform that combines a eukaryotic expression vector with live, highly attenuated *Salmonella* as the delivery system. Based on COBRA, virus-like particles have been produced by selecting a specific time interval, and those particles have been reported to elicit broadly reactive neutralizing antibodies that can neutralize multiple influenza strains and protect mice, ferrets, and nonhuman primates against a viral challenge from the H1N1, H3N2, and H5N1 subtypes [12,13,37,38]. HA1 forms a trimer that displays antigenic sites at the distal tip of each subunit. Through its secondary structure, the RBS is responsible for binding with a sialic acid receptor of the host. Five immunodominant antigenic sites, Sa (residues 128–129, 156–160, 162–167 AA), Sb (residues 187–198 AA), Ca1 (residues 169–173, 206–208, 238–240 AA), Ca2 (residues 140–145, 224–225 AA), and Cb (residues 74–79 AA), are located on the globular portion and are important for stimulating an immune response against the influenza virus [39]. Sa and Sb are strain-specific sites near the spike tip, and the RBS is a highly mutable hotspot, leading to antigenic drift. The C sites, located further down, are less variable and exhibit cross-reactivity. Antigenic variation in HA favors escape from neutralization by antibodies induced by a vaccine or prior infection. Therefore, we designed vaccine constructs that cover different portions of the globular head region of H1N1. Construct #5, which encodes the globular

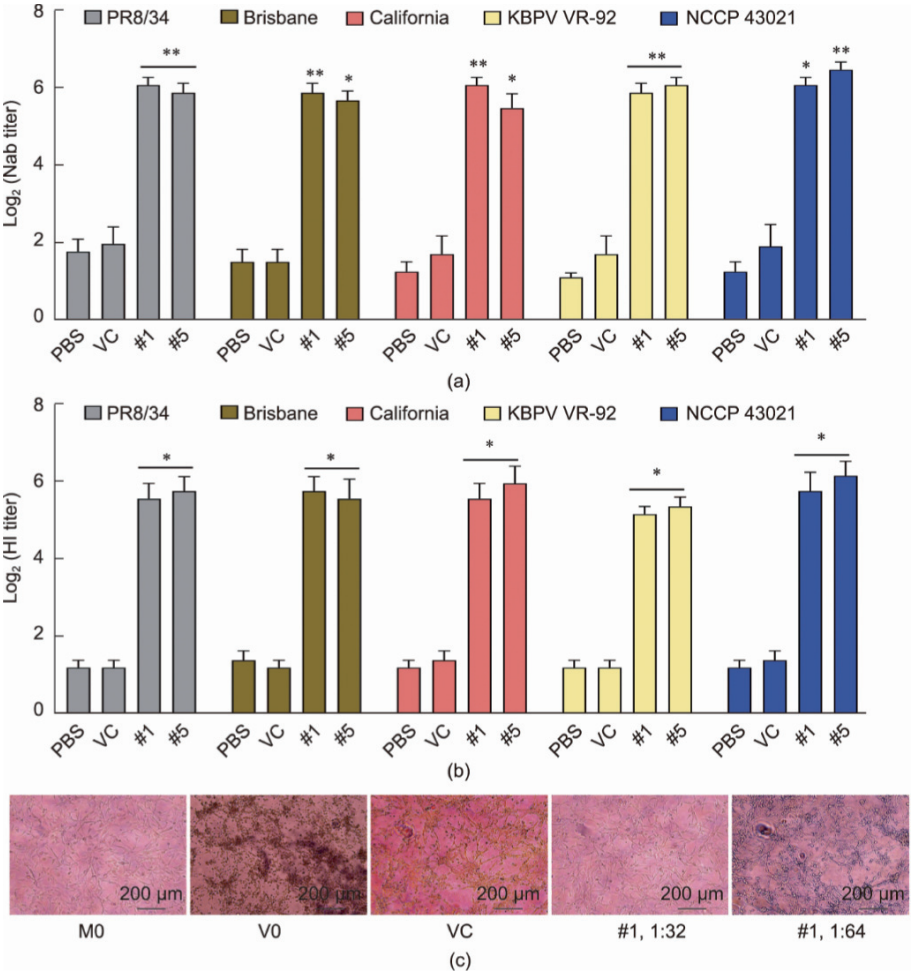

Fig. 7. Evaluation of protection from influenza virus. (a) Neutralization assay of sera from immunized mice. Sera were collected 21 dpi, and the NAb titer was measured in MDCK cells as inhibition of CPE at maximum dilution. The NAb titer was evaluated for selected construct strains. (b) Serum HI titers. A serial twofold dilution of heat-inactivated serum was treated with four HA unit equivalents of the virus, and HI was assessed using chicken erythrocytes. (c) Representative images of the MN assay illustrating the inhibition of CPE at different serum dilutions. MO: media only, VO: virus only. Data were analyzed by Dunnett's multiple comparisons test and ANOVA. $^{*}P < 0.05$ and $^{**}P < 0.01$.

head region of HA from 1 to 300 AA, was selected as the full-length construct. Construct #1 covers the core region of the RBS from 90 to 240 AA, targeting the binding pockets in the 127–235 AA sequence. In construct #1, glycosylation sites were exempted except at 95 AA, which is found in almost all H1N1 viruses.

The presence of glycans on HA shields antigenic sites from immune recognition and reduces its affinity for receptors [40,41]. Such a shielding effect has been reported in enveloped viruses such as human immunodeficiency virus [42]. Considering that the non-glycosylated HA globular head region is expected to elicit a more potent antibody response, and HA globular head folding can form protein crystals without other glycosylation sites [43], we designed construct #1 to have minimal glycosylation sites. Previous studies have reported that a similar non-glycosylated form of the HA-receptor-binding domain (RBD;63–286 AA) exhibited spontaneous refolding into its native immunogenic structure, maintaining intact epitopes and a functional receptor-binding pocket [44]. Thus, the selected construct was expected to undergo spontaneous folding and form a stable antigen protein structure. We found that construct #1, which lacks a glycosylated region except at 95 AA, offered consistent and effective immunity. This finding aligns with previous findings in ferrets [44,45]. It is worth noting that seasonal human H1N1 influenza viruses typically possess four or five glycosylation sites in their HA-RBDs, whereas the HA-RBD of the 1918 H1N1 Spanish flu pandemic virus and the 2009 swine-origin H1N1 pandemic virus feature only a single glycosylation site [11]. An in silico analysis to assess the structural integrity of the strategically designed consensus sequences (#1 to #5), as well as the absence of outliers in the Ramachandran plot, validate the reliability of these constructs (Fig. 2(a)).

We used a *Salmonella* delivery system in combination with a specific eukaryotic expression vector, pJHL204, to ensure the successful delivery of DNA and the expression of the desired antigen [21]. This RdRp-dependent eukaryotic expression system enhances antigen expression via cytoplasmic mRNA amplification. The vaccine constructs were delivered using live-attenuated *Salmonella*, and both murine (RAW 267.4) and human (HEK293T) cell lines exhibited mRNA expression after bactofection (Figs. 3(a) and (b)). Herein, we provide the proof of concept for *Salmonella*-mediated in vitro expression of a recombinant protein, as shown by our western blotting and IFA results (Figs. 3(c) and (d)). This suggests the suitability of using attenuated *Salmonella* with a eukaryotic expression vector to confer antigenic expression from the consensus sequence. The production of NAbs against the vaccine constructs reinforces the functional characteristics of the expressed antigens [46]. We also evaluated the safety of the vaccine construct in mice. Our construct produced minimal inflammation in the spleen and liver for a short period after immunization, which also

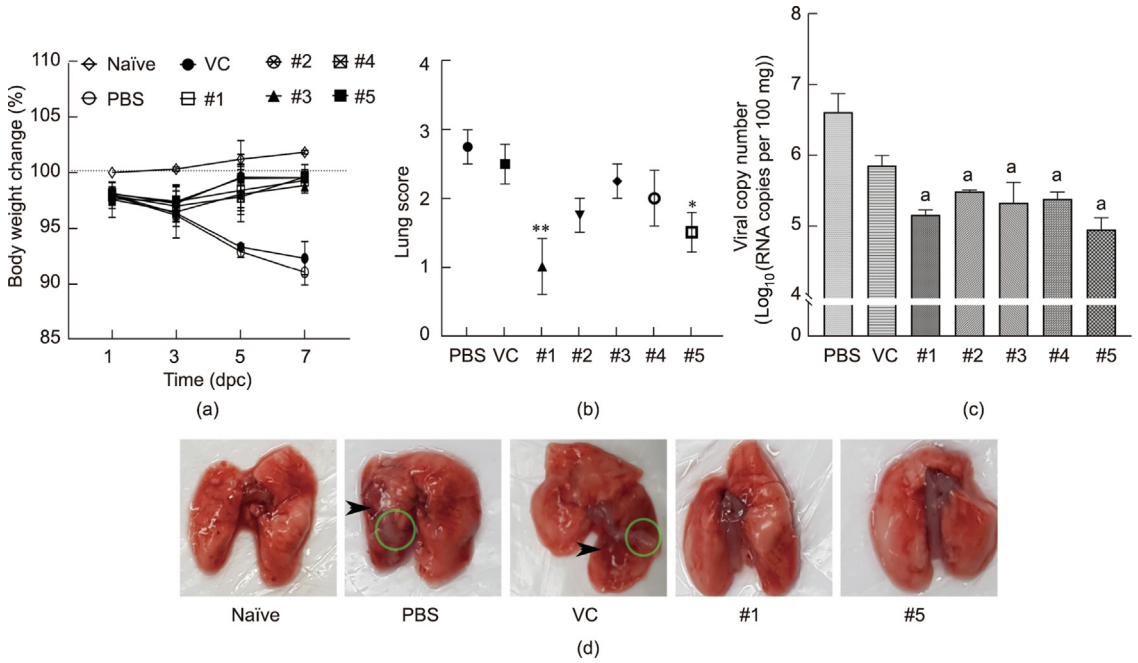

Fig. 8. Evaluation of protection from influenza A PR8/34 virus. (a) Body weight changes were monitored up to 7 days post-challenge (dpc). The weight of the mice on day 0 was taken as the reference for the comparative percentage of body weight loss post-challenge. (b) Morphological disease severity score index for the lungs. Lungs were harvested 3 dpc and examined for morphological changes. The gross analysis of harvested lungs rated disease severity based on the lungs of naïve mice as control and was scored as 0 for no change, and 1 to 3 as mild, moderate, and severe complications, respectively. * and ** indicate significant difference from the non-immunized group at a significance of $P < 0.05$ and $P < 0.01$ respectively. (c) The viral copy number in lung tissue was evaluated 3 dpc. A letter indicates statistically significant difference from the non-immunized control group while the same letter indicates no significant difference among the groups. Data were analyzed by Dunnett's multiple comparisons test. (d) Selected images showing morphological changes with different lung index scores post-challenge. The arrowhead denotes dark lesions, and the green circle illustrates edema. Lung index score for naïve = 0, PBS = 3, VC = 2, #1 = 1, and #5 = 1.

indicates an immune response (Fig. 4(b)). The clearance of *Salmonella* from the spleen and liver in the second week post-infection confirms the safety of the vaccine candidate [28].

The induction of an early adaptive humoral response facilitates the clearance of invading H1N1 influenza virus during the initial phase of infection [47]. To investigate whether such a response occurred, we monitored the levels of IgG elicited by immune response priming (Fig. 5(a)). Furthermore, we examined subclasses of IgG and found that the production of IgG2a was higher than that of IgG1 (Fig. 5(b)). This observation suggests a Th1-dominant cell-mediated response, and such an inclination toward a Th1 immune response deciphers the paradigm of the intracellular antiviral response [48]. Cell-mediated immunity (CMI) plays a vital role in host protection against intracellular pathogens. It has been reported that an increase in H1N1 influenza A virus-specific CD4 and CD8 T cells lowers the infection rate [49], and we observed a prominent increase in both T cells after vaccination with constructs #1 and #5 (Fig. 5(d)), which demonstrates the induction of CMI as a protective response post-vaccination. Construct #2 carries glycosylated regions, and glycosylated viral proteins and processed epitopes are infrequently targeted by T cells [50], inhibiting T cell recognition and altering T cell immunity against viral infection. In addition, HA proteins with single *N*-glycans were more effective than complex-type *N*-glycans in triggering mouse dendritic cell activation and maturation [51]. This supports the idea that simpler glycosylation, as in construct #1, is effective in triggering an immune response. Of note, construct #3 might not have an antigenic presentation that properly stimulates an immune response. We evaluated the Th1-related cytokine IFN-γ to support our finding of antiviral activity, and the induction of antiviral defenses through an antibody response was also reflected by the Th2-related cytokine IL-4. Generally, IL-10 indicates a Th2 response; specifically, during influenza infection, it is produced by $CD4^+$ effector T cells and $CD8^+$ T cells to limit excessive inflammation [52,53]. A significant increase in IL-17 implies the activation of Th17 cells that are associated with modulating inflammation and clearing influenza infection at the mucosal barrier [54].

The antiviral activity of IFN-γ is well established, and its effects on lung epithelial cells inhibit influenza virus amplification [55,56]. Active T helper cells ($CD4^+$) produce IFN-γ to recruit immune cells and stimulate the differentiation of B lymphocytes to clear viral infection, whereas cytotoxic T cells ($CD8^+$) produce IFN-γ to directly kill and eradicate viral particles and infected cells. Thus, the demonstration of higher production of $CD4^+$IFN-γ^+ and $CD8^+$IFN-γ^+ T cells after immunization with construct #5 or #1 illustrates that immunization induced a pronounced antiviral effect. In addition, the stimulation of B cell proliferation and isotype switching is essential to produce immunoglobulins, and Th2 type cells produce IL-4 for that purpose [57]. The substantial production of $CD4^+$IL-4^+ T cells found in the immunized mice aids in B cell proliferation [58]. This confirmed the induction of a humoral response by constructs #1 and #5.

The functional characteristics of antigens delivered via immunization are assessed by the production of NAbs [46]. Therefore, the presence of NAbs in the immunized groups was evaluated to determine the antiviral response. The MN titer recorded for constructs #1 and #5 was in the range of a $\log_2$(NAb titer) of 6.0 for the tested virus strains (Fig. 7(a)). In previous reports, an MN titer of 1:40 against influenza A conferred 49% protection against PCR-confirmed cases [59] Thus the concentration of NAbs generated in our immunized mice was sufficient to protect them against H1N1 infection. An HI titer of $\geq$ 40 is generally accepted as a threshold indicating immunity [60]. Both constructs elicited an HI titer higher than that threshold value for all the tested virus strains, indicating the induction of protective immunity

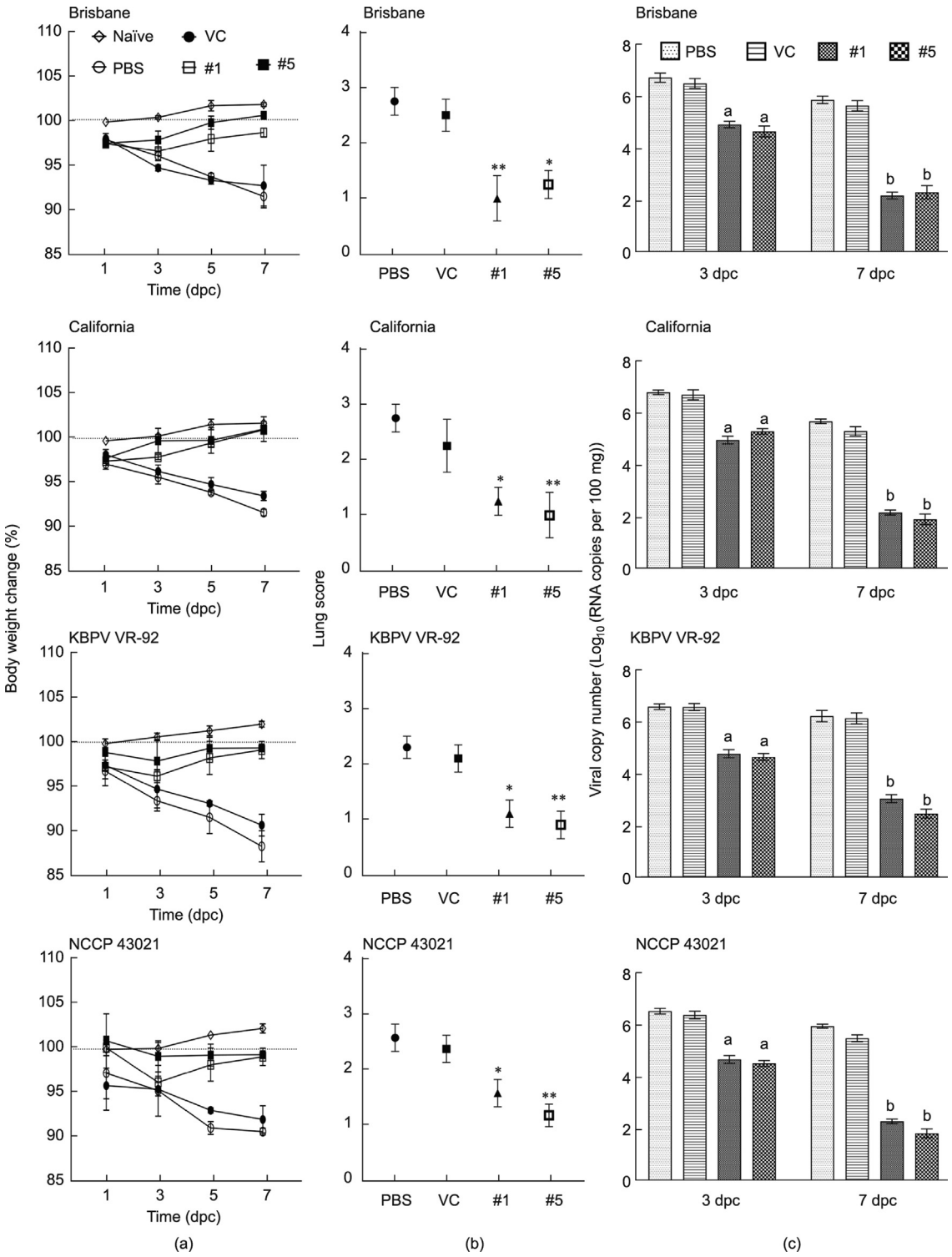

Fig. 9. Evaluation of protection from several influenza A virus strains: A/Brisbane/59/2007, A/California/07/2009, KBPV VR-92, and NCCP 43021. (a) Body weight changes. (b) Morphological disease severity score index for lungs. Lung scores, 0: no change, 1: mild, 2: moderate, and 3: severe. (c) Viral copy number in lung tissue. Different letters indicate statistically significant differences from the non-immunized control group and among different time points. Data were analyzed by Dunnett's multiple comparisons test and ANOVA. $^{*}P < 0.05$ and $^{**}P < 0.01$. Letters indicate statistically significant difference from the non-immunized control group. Different letters, a, b, signify significant differences among the groups.

(Fig. 7(b)). In addition, the similar titer value for virus neutralization and HI indicates the positive correlation between them, which is consistent with a published report [61].

The broad spectral protection provided by the consensus sequence designed by COBRA was thoroughly tested across various H1N1 strains of the influenza A virus. The strain selection was based on their prevalence in both past and current circulating outbreaks. To ensure a comprehensive evaluation, three global strains were chosen to represent widespread geographical locations, and two additional local strains were isolated. The effectiveness of

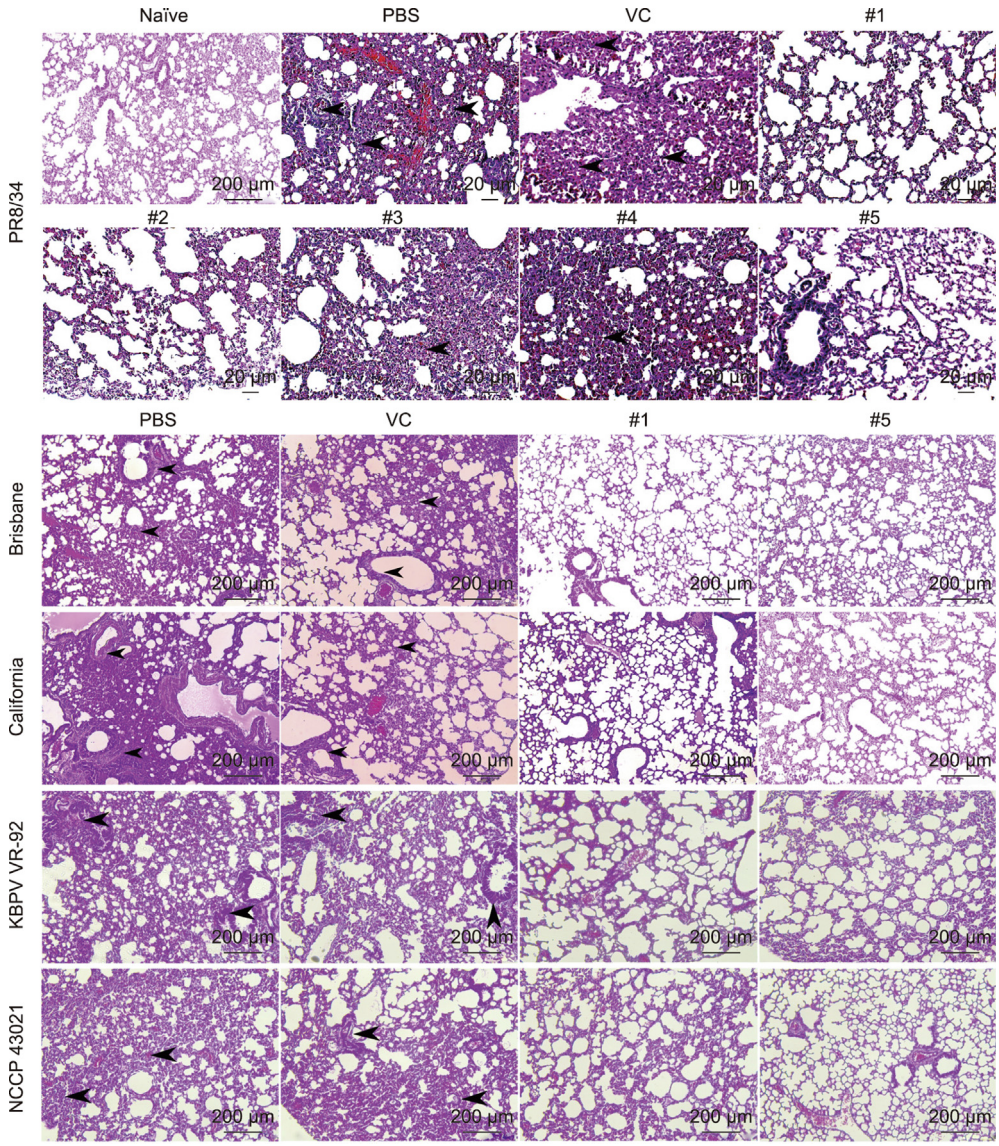

Fig. 10. Assessment of the protective immune response on lung pathology. Histopathological deformation observed in lung sections by H&E staining of tissue sections challenged with influenza A/PR/8/434, A/Brisbane/59/2007, A/California/07/2009, KBPV VR-92, and NCCP 43021. Remarkable inflammation and the presence of perivascular and peribronchial infiltrates were noted in the non-immunized and VC groups. Alveolar congestion with thick alveolar septa and alveolar collapse, along with cell debris in the bronchiolar lumen, are denoted by arrowheads in the non-immunized and VC groups. Alveolar congestion was limited in the vaccinated groups.

the protection offered by immunization was demonstrated through minimal body weight loss and low severity score indexes for the lungs compared with the control group (Figs. 8 and 9) because an increase in alveolar collapse is an indication of severe infection with influenza A virus [62]. The protection efficacy was confirmed by the low viral copy number found in immunized mice through the qRT-PCR analysis. Mice challenged with the influenza A/PR/8/34 strain showed negligible morphological changes in the lungs and a significant decrease in viral copy number, especially with constructs #1 and #5. Consequently, only these two constructs were evaluated for their ability to protect against other virus strains. Both constructs produced a prominent drop in viral load at 7 days post-challenge with the influenza A/Brisbane/59/2007, A/California/07/2009, KBPV VR-92, and NCCP 43021 strains, which is clear evidence of better protection. The histopathological analysis revealed minor inflammation in mice immunized with constructs #1 and #5. In contrast, we found remarkable inflammation in the epithelia of the larger airways, along with the presence of perivascular and peribronchial infiltration of leucocytes in the control and VC groups. Moreover, alveolar congestion in the non-immunized and VC groups was clear evidence of tissue distortion caused by infection (Fig. 10). This study thus clearly demonstrates that immunization with the COBRA-derived consensus sequence effectively reduced the severity of lung infections, lowered viral replication, and mitigated the inflammation and tissue damage associated with a broad spectrum of H1N1 viral challenges. Therefore, the COBRA approach is appropriate for the development of a highly effective vaccine against influenza A virus infections.

In conclusion, we used COBRA to resolve the issue of antigenic variation and yearly vaccine reformulation by constructing a consensus sequence of the HA1 region of the H1N1 influenza virus. We demonstrated in vivo gene delivery of the designed constructs using a eukaryotic expression vector and an attenuated *Salmonella* delivery system. This strategy produced robust humoral and CMI responses, offering broad spectral protection against five H1N1 influenza strains (A/PR8/34, A/Brisbane/59/2007, A/California/07/2009, KBPV VR-92, and NCCP 43021) in a mouse model. By

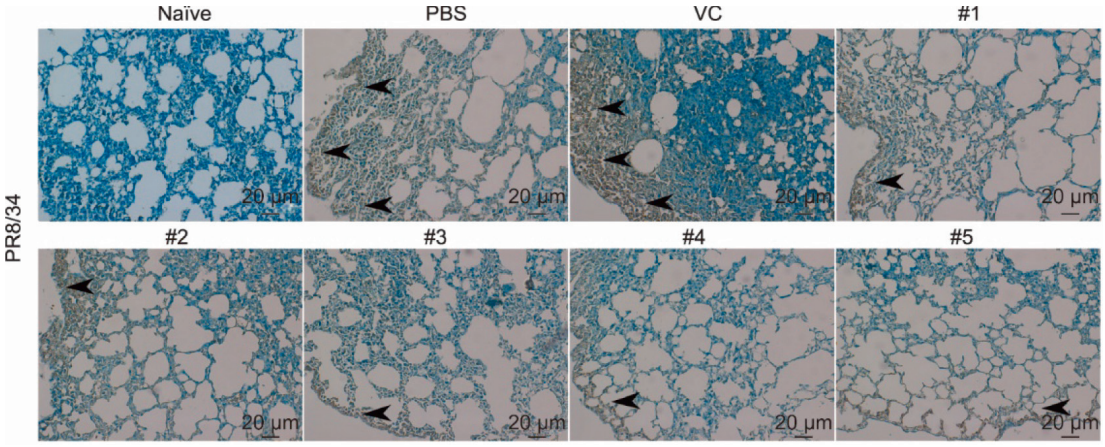

Fig. 11. Localization of viral particles stained in an IHC assay. Lung tissue sections challenged with influenza A/PR/8/34 were stained with rabbit anti-recombinant protein polyclonal antibodies to illustrate the localization of the virus. Brown spots indicate foci of viral infection stained with DAB.

using *Salmonella* as a delivery system, we not only eliminated the need for yearly reformulation but also ensured the capacity for rapid production during outbreaks when time is of the essence.

Acknowledgments

This Work was supported by Basic Science Research Program through the National Research Foundation of Korea (NRF) funded by the Ministry of Education (2019R1A6A1A03033084).

Compliance with ethics guidelines.

All animal experiments performed in this study were according to the methods approved by the Jeonbuk National University Animal Ethics Committee (JBNU-2021-027) under the guidelines of the Korean Council on animal care and the Korean Animal Protection Law, 2007: Article 13.

Ram Prasad Aganja, Amal Senevirathne, Chandran Sivasankar, and John Hwa Lee declare that they have no conflict of interest or financial conflicts to disclose.

Appendix A. Supplementary material

Supplementary data to this article can be found online at https://doi.org/10.1016/j.eng.2023.08.001.

References

[1] Fraser C, Donnelly CA, Cauchemez S, Hanage WP, van Kerkhove MD, Hollingsworth TD, et al.; WHO Rapid Pandemic Assessment Collaboration. Pandemic potential of a strain of influenza A (H1N1): early findings. Science 2009;324(5934):1557–61.
[2] Horimoto T, Kawaoka Y. Influenza: lessons from past pandemics, warnings from current incidents. Nat Rev Microbiol 2005;3(8):591–600.
[3] Xing L, Chen Y, Chen B, Bu L, Liu Y, Zeng Z, et al. Antigenic drift of the hemagglutinin from an influenza A (H1N1) pdm09 clinical isolate increases its pathogenicity *in vitro*. Virol Sin 2021;36(5):1220–7.
[4] McLean HQ, Belongia EA. Influenza vaccine effectiveness: new insights and challenges. Cold Spring Harb Perspect Med 2021;11(6):a038315.
[5] Shim BS, Choi YK, Yun CH, Lee EG, Jeon YS, Park SM, et al. Sublingual immunization with M2-based vaccine induces broad protective immunity against influenza. PLoS One 2011;6(11):e27953.
[6] Andersson AM, Håkansson KO, Jensen BA, Christensen D, Andersen P, Thomsen AR, et al. Increased immunogenicity and protective efficacy of influenza M2e fused to a tetramerizing protein. PLoS One 2012;7(10):e46395.
[7] Sangster MY, Nguyen PQT, Topham DJ. Role of memory B cells in hemagglutinin-specific antibody production following human influenza A virus infection. Pathogens 2019;8(4):167.
[8] Copeland CS, Doms RW, Bolzau EM, Webster RG, Helenius A. Assembly of influenza hemagglutinin trimers and its role in intracellular transport. J Cell Biol 1986;103(4):1179–91.
[9] Weis W, Brown JH, Cusack S, Paulson JC, Skehel JJ, Wiley DC. Structure of the influenza virus haemagglutinin complexed with its receptor, sialic acid. Nature 1988;333(6172):426–31.
[10] Wilson IA, Skehel JJ, Wiley DC. Structure of the haemagglutinin membrane glycoprotein of influenza virus at 3 A resolution. Nature 1981;289 (5796):366–73.
[11] Das SR, Puigbò P, Hensley SE, Hurt DE, Bennink JR, Yewdell JW. Glycosylation focuses sequence variation in the influenza A virus H1 hemagglutinin globular domain. PLoS Pathog 2010;6(11):e1001211.
[12] Giles BM, Ross TM. A computationally optimized broadly reactive antigen (COBRA) based H5N1 VLP vaccine elicits broadly reactive antibodies in mice and ferrets. Vaccine 2011;29(16):3043–54.
[13] Carter DM, Darby CA, Lefoley BC, Crevar CJ, Alefantis T, Oomen R, et al. Design and characterization of a computationally optimized broadly reactive hemagglutinin vaccine for H1N1 influenza viruses. J Virol 2016;90 (9):4720–34.
[14] Wong TM, Allen JD, Bebin-Blackwell AG, Carter DM, Alefantis T, DiNapoli J, et al. Computationally optimized broadly reactive hemagglutinin elicits hemagglutination inhibition antibodies against a panel of H3N2 influenza virus cocirculating variants. J Virol 2017;91(24):e01581–10617.
[15] Chen J, Wang J, Zhang J, Ly H. Advances in development and application of influenza vaccines. Front Immunol 2021;12:711997.
[16] Skowronski DM, Janjua NZ, De Serres G, Sabaiduc S, Eshaghi A, Dickinson JA, et al. Low 2012–13 influenza vaccine effectiveness associated with mutation in the egg-adapted H3N2 vaccine strain not antigenic drift in circulating viruses. PLoS One 2014;9(3):e92153.
[17] Kirthika P, Senevirathne A, Jawalagatti V, Park S, Lee JH. Deletion of the lon gene augments expression of *Salmonella* pathogenicity island (SPI)-1 and metal ion uptake genes leading to the accumulation of bactericidal hydroxyl radicals and host pro-inflammatory cytokine-mediated rapid intracellular clearance. Gut Microbes 2020;11(6):1695–712.
[18] Brumell JH, Goosney DL, Finlay BB. SifA, a type III secreted effector of *Salmonella typhimurium*, directs *Salmonella*-induced filament (Sif) formation along microtubules. Traffic 2002;3(6):407–15.
[19] Kong W, Brovold M, Koeneman BA, Clark-Curtiss J, Curtiss R 3rd. Turning self-destructing *Salmonella* into a universal DNA vaccine delivery platform. PNAS 2012;109(47):19414–9.
[20] Ng KK, Arnold JJ, Cameron CE. Structure-function relationships among RNA-dependent RNA polymerases. Curr Top Microbiol Immunol 2008;320:137–56.
[21] Senevirathne A, Park JY, Hewawaduge C, Perumalraja K, Lee JH. Eukaryotic expression system complemented with expressivity of Semliki Forest virus's RdRp and invasiveness of engineered *Salmonella* demonstrate promising potential for bacteria mediated gene therapy. Biomaterials 2021;279:121226.
[22] Liljeström P, Garoff H. A new generation of animal cell expression vectors based on the Semliki Forest virus replicon. Biotechnology 1991;9(12):1356–61.
[23] Bao Y, Bolotov P, Dernovoy D, Kiryutin B, Zaslavsky L, Tatusova T, et al. The influenza virus resource at the National Center for Biotechnology Information. J Virol 2008;82(2):596–601.
[24] Gopalakrishnan K, Sowmiya G, Sheik SS, Sekar K. Ramachandran plot on the web (2.0). Protein Pept Lett 2007;14(7):669–71.
[25] Larsen JE, Lund O, Nielsen M. Improved method for predicting linear B-cell epitopes. Immunome Res 2006;2(1):2.
[26] Kozakov D, Hall DR, Xia B, Porter KA, Padhorny D, Yueh C, et al. The ClusPro web server for protein-protein docking. Nat Protoc 2017;12(2):255–78.
[27] Ramírez-Aportela E, López-Blanco JR, Chacón P. FRODOCK 2.0: fast protein-protein docking server. Bioinformatics 2016;32(15):2386–8.

[28] Aganja RP, Sivasankar C, Hewawaduge C, Lee JH. Safety assessment of compliant, highly invasive, lipid A-altered, O-antigen-defected *Salmonella* strains as prospective vaccine delivery systems. Vet Res 2022;53(1):76.
[29] Kruisbeek AM. Isolation of mouse mononuclear cells. Curr Protoc Immunol 2001; Chapter 3:Unit 3.1.
[30] Denizot F, Lang R. Rapid colorimetric assay for cell growth and survival. Modifications to the tetrazolium dye procedure giving improved sensitivity and reliability. J Immunol Methods 1986;89(2):271–7.
[31] Hajam IA, Lee JH. Preexisting *Salmonella*-specific immunity interferes with the subsequent development of immune responses against the *Salmonella* strains delivering H9N2 hemagglutinin. Vet Microbiol 2017;205:117–23.
[32] Pfaffl MW. A new mathematical model for relative quantification in real-time RT-PCR. Nucleic Acids Res 2001;29(9):e45.
[33] Laurie KL, Engelhardt OG, Wood J, Heath A, Katz JM, Peiris M, et al.; CONSISE Laboratory Working Group participants. International laboratory comparison of influenza microneutralization assays for A(H1N1) pdm09, A(H3N2), and A (H5N1) influenza viruses by CONSISE. Clin Vaccine Immunol 2015;22 (8):957–64.
[34] WHO. Manual for the laboratory diagnosis and virological surveillance of influenza. Geneva: WHO; 2011.
[35] Song HO, Kim JH, Ryu HS, Lee DH, Kim SJ, Kim DJ, et al. Polymeric LabChip real-time PCR as a point-of-care-potential diagnostic tool for rapid detection of influenza A/H1N1 virus in human clinical specimens. PLoS One 2012;7(12): e53325.
[36] Kleywegt GJ, Jones TA. Phi/psi-chology: Ramachandran revisited. Structure 1996;4(12):1395–400.
[37] Giles BM, Crevar CJ, Carter DM, Bissel SJ, Schultz-Cherry S, Wiley CA, et al. A computationally optimized hemagglutinin virus-like particle vaccine elicits broadly reactive antibodies that protect nonhuman primates from H5N1 infection. J Infect Dis 2012;205(10):1562–70.
[38] Carter DM, Darby CA, Johnson SK, Carlock MA, Kirchenbaum GA, Allen JD, et al. Elicitation of protective antibodies against a broad panel of H1N1 viruses in ferrets preimmune to historical H1N1 influenza viruses. J Virol 2017;91(24): e01283–10317.
[39] Sriwilaijaroen N, Suzuki Y. Molecular basis of the structure and function of H1 hemagglutinin of influenza virus. Proc Jpn Acad Ser B Phys Biol Sci 2012;88 (6):226–49.
[40] Schulze IT. Effects of glycosylation on the properties and functions of influenza virus hemagglutinin. J Infect Dis 1997;176(Suppl 1):S24–8.
[41] Abe Y, Takashita E, Sugawara K, Matsuzaki Y, Muraki Y, Hongo S. Effect of the addition of oligosaccharides on the biological activities and antigenicity of influenza A/H3N2 virus hemagglutinin. J Virol 2004;78(18):9605–11.
[42] Kubo Y, Yokoyama M, Yoshii H, Mitani C, Tominaga C, Tanaka Y, et al. Inhibitory role of CXCR4 glycan in CD4-independent X4-tropic human immunodeficiency virus type 1 infection and its abrogation in CD4-dependent infection. J Gen Virol 2007;88(Pt 11):3139–44.
[43] Xuan C, Shi Y, Qi J, Zhang W, Xiao H, Gao GF. Structural vaccinology: structure-based design of influenza A virus hemagglutinin subtype-specific subunit vaccines. Protein Cell 2011;2(12):997–1005.
[44] DuBois RM, Aguilar-Yañez JM, Mendoza-Ochoa GI, Oropeza-Almazán Y, Schultz-Cherry S, Alvarez MM, et al. The receptor-binding domain of influenza virus hemagglutinin produced in *Escherichia coli* folds into its native, immunogenic structure. J Virol 2011;85(2):865–72.
[45] Aguilar-Yáñez JM, Portillo-Lara R, Mendoza-Ochoa GI, García-Echauri SA, López-Pacheco F, Bulnes-Abundis D, et al. An influenza A/H1N1/2009 hemagglutinin vaccine produced in Escherichia coli. PLoS One 2010;5(7): e11694.
[46] Wu NC, Wilson IA. Structural insights into the design of novel anti-influenza therapies. Nat Struct Mol Biol 2018;25(2):115–21.
[47] Qiu C, Tian D, Wan Y, Zhang W, Qiu C, Zhu Z, et al. Early adaptive humoral immune responses and virus clearance in humans recently infected with pandemic 2009 H1N1 influenza virus. PLoS One 2011;6(8):e22603.
[48] Tamura S, Miyata K, Matsuo K, Asanuma H, Takahashi H, Nakajima K, et al. Acceleration of influenza virus clearance by Th1 cells in the nasal site of mice immunized intranasally with adjuvant-combined recombinant nucleoprotein. J Immunol 1996;156(10):3892–900.
[49] Tsang TK, Lam KT, Liu Y, Fang VJ, Mu X, Leung NHL, et al. Investigation of CD4 and CD8 T cell-mediated protection against influenza A virus in a cohort study. BMC Med 2022;20(1):230.
[50] Olvera A, Cedeño S, Llano A, Mothe B, Sanchez J, Arsequell G, et al. Does antigen glycosylation impact the HIV-specific T cell immunity? Front Immunol 2021;11:573928.
[51] Liu WC, Lin YL, Spearman M, Cheng PY, Butler M, Wu SC. Influenza virus hemagglutinin glycoproteins with different *N*-glycan patterns activate dendritic cells in vitro. J Virol 2016;90(13):6085–96.
[52] Sun J, Madan R, Karp CL, Braciale TJ. Effector T cells control lung inflammation during acute influenza virus infection by producing IL-10. Nat Med 2009;15 (3):277–84.
[53] Jiang L, Yao S, Huang S, Wright J, Braciale TJ, Sun J. Type I IFN signaling facilitates the development of IL-10-producing effector CD8+ T cells during murine influenza virus infection. Eur J Immunol 2016;46(12): 2778–88.
[54] Antalis E, Spathis A, Kottaridi C, Kossyvakis A, Pastellas K, Tsakalos K, et al. Th17 serum cytokines in relation to laboratory-confirmed respiratory viral infection: a pilot study. J Med Virol 2019;91(6):963–71.
[55] Seo SH, Webster RG. Tumor necrosis factor alpha exerts powerful anti-influenza virus effects in lung epithelial cells. J Virol 2002;76(3):1071–6.
[56] Bot A, Bot S, Bona CA. Protective role of gamma interferon during the recall response to influenza virus. J Virol 1998;72(8):6637–45.
[57] Rush JS, Hodgkin PD. B cells activated via CD40 and IL-4 undergo a division burst but require continued stimulation to maintain division, survival and differentiation. Eur J Immunol 2001;31(4):1150–9.
[58] Noma T. Function, molecular structure and gene expression of IL-4. Nihon Rinsho 1992;50(8):1787–94. Japanese.
[59] Tsang TK, Cauchemez S, Perera RA, Freeman G, Fang VJ, Ip DK, et al. Association between antibody titers and protection against influenza virus infection within households. J Infect Dis 2014;210(5):684–92.
[60] Cox RJ. Correlates of protection to influenza virus, where do we go from here? Hum Vaccin Immunother 2013;9(2):405–8.
[61] Truelove S, Zhu H, Lessler J, Riley S, Read JM, Wang S, et al. A comparison of hemagglutination inhibition and neutralization assays for characterizing immunity to seasonal influenza A. Influenza Other Respi Viruses 2016;10 (6):518–24.
[62] Fukushi M, Ito T, Oka T, Kitazawa T, Miyoshi-Akiyama T, Kirikae T, et al. Serial histopathological examination of the lungs of mice infected with influenza A virus PR8 strain. PLoS One 2011;6(6):e21207.